Emerging Spintronic Materials and Functionalities

Lidan Guo, Shunhua Hu, Xianrong Gu, Rui Zhang, Kai Wang*, Wenjing Yan* and Xiangnan Sun**

L. Guo, S. Hu, X. Gu, R. Zhang, X. Sun
Key Laboratory of Nanosystem and Hierarchical Fabrication, National Center for Nanoscience and Technology, Beijing 100190, P. R. China
E-mail: guxr@nanoctr.cn; sunxn@nanoctr.cn

S. Hu, X. Sun
Center of Materials Science and Optoelectronics Engineering, University of Chinese Academy of Sciences, Beijing 100049, P. R. China

K. Wang
Key Laboratory of Luminescence and Optical Information, Ministry of Education, School of Physical Science and Engineering, Institute of Optoelectronics Technology, Beijing Jiaotong University, Beijing, 100044, P. R. China
E-mail: kaiwang@bjtu.edu.cn

W. Yan
School of Physics and Astronomy, University of Nottingham, University Park, Nottingham, NG9 2RD, United Kingdom
E-mail: wenjing.yan@nottingham.ac.uk

X. Sun
School of Material Science and Engineering, Zhengzhou University, Zhengzhou 450001, P. R. China

Keywords: organic semiconductors, organic-inorganic hybrid perovskites, two-dimensional materials, chiral-induced spin selectivity, multifunctional spintronic devices

Abstract

The explosive growth of the information era has put forward urgent requirements for ultra-high-speed and extremely efficient computations. In direct contrary to charge-based computations, spintronics aims to use spins as information carriers for data storage, transmission, and decoding, to help fully realize electronic device miniaturization and high integration for next-generation computing technologies. Currently, many novel spintronic materials have been developed with unique properties and multi-functionalities, including organic semiconductors (OSCs), organic-inorganic hybrid perovskites (OIHPs), and two-dimensional materials (2DMs). These materials are useful to fulfil the demand for developing diverse and advanced spintronic devices. Herein, we systematically reviewed these promising materials for advanced spintronic applications. Due to the distinct chemical and physical structures of OSCs, OIHPs, and 2DMs, their spintronic properties (spin transport and spin manipulation) were discussed separately. In addition, some multifunctionalities due to photoelectric and chiral-induced spin selectivity (CISS) were overviewed, including the spin-filter effect, spin-photovoltaics, spin-light emitting devices, and spin-transistor functions. Subsequently, we presented challenges and future perspectives of using these multifunctional materials for the development of advanced spintronics.

1. Introduction

The discovery of giant magnetoresistance (GMR) and its applications in magnetic sensors[1] has triggered the utilization of spins as information carriers and quantum bits for data storage and transmission.[2] Since then, the study of spins has become increasingly important under the fast growths of material science, nanotechnology, quantum and topological physics,[3] and a new interdisciplinary research field known as spintronics was established.[1c, 4] One of the ultimate goals of this field is to obtain efficient spin-polarized electronic transport[5] and spin manipulation[2e, 6] in solid-state materials. Various functional materials for high-performance spintronic applications have been successfully synthesized from inorganic semiconductors[3q, 7] to organic semiconductors (OSCs).[8] Over the past decade, spintronics has attracted growing interest in organic-inorganic hybrid perovskites (OIHPs)[3s, 9] and two-dimensional materials (2DMs).[10] Thus, a thorough understanding of these different multifunctional material systems, and their correlation, is critically important for the future development of advanced and efficient spintronic devices.

In principle, the spin transport properties of a given material can be evaluated by the spin diffusion length (λ) and the spin lifetime (τ), which can be correlated with the spin diffusion constant (D) as follows:

$$\lambda = \sqrt{D\tau}\,, \tag{1}$$

where D is material dependent. To sustain remarkable spin polarization during spin transport and manipulation in a material, a long λ and a large τ are desirable. Nevertheless, spin dephasing cannot be avoided in reality[11] and will vary significantly for different material systems because of their different chemical constituents, structures, and dimensionalities. One of the most significant contributions is spin-orbit coupling (SOC).[12] It is indeed a relativistic effect and originates from the interaction of the spin angular momentum with the orbital angular momentum of an electron. SOC is also considered proportional to the fourth power of an atomic number for a chemical element. In addition, an externally applied magnetic field (B) can interfere with the spin angular momentum, leading to spin precession. The precession rate is also known as the Lamor frequency (ω_{L}), can be expressed as follows:

$$\omega_{\mathrm{L}} = g\mu_{\mathrm{B}}B/\hbar\,, \tag{2}$$

where μ_{B} is the Bohr magneton, $\hbar$ is the Planck's constant and g denotes the Landá-g factor with its magnitude determining the SOC strength, and consequently, ω_{L} is also linked to SOC. Moreover, the one-dimensional spin drift-diffusion model can describe the combined effect of spin diffusion, precession, and relaxation, and can be expressed as follows:

$$\Delta R\left(B_{\mathrm{Z}}\right) \propto \int_0^{\infty} \frac{1}{\sqrt{4\pi Dt}} \exp\left(-\frac{d^2}{4Dt}\right) \cos\left(\omega_{\mathrm{L}} t\right) \exp\left(-\frac{t}{\tau}\right) \mathrm{dt} \quad , \qquad (3)$$

where d is the thickness of the spacer, t is time, ΔR is the resistance difference as a result of the changing perpendicular magnetic field B_z.[9b] According to equations (2) and (3), λ and τ can be extracted from the measured spin precession data. Despite this, other spin-associated phenomena such as hyperfine interaction (HFI)[13] and the Bychkov-Rashba effect[14] also have pronounced impacts on spin transport and manipulation. HFI refers to the interaction between the nuclear spin and the magnetic field produced by the electrons, while the Bychkov-Rashba effect refers to the splitting of electronic energy levels in materials with strong SOC. All of these effects are material dependent, and some may even coexist and be jointly responsible for spin transport and manipulation in the three aforementioned systems.

Among the three classes of material systems, most amorphous OSCs have relatively weak SOC strengths and long spin lifetimes due to the presence of light chemical elements.[8f] As a result, large spin valve-based magnetoresistance (SV-MR) and tunneling magnetoresistance (TMR) have been achieved.[15] On the contrary, many crystalline OIHPs possess relatively strong SOC due to the presence of heavy elements, such as lead (Pb) and iodine (I).[16] Due to structure inversion asymmetry (SIA), they also exhibit the Rashba effect,[17] leading to spin-related energy level degeneracies in momentum vector spaces. Many newly raised chiral perovskites and molecules also possess remarkable chiral-induced SOC because of their structural helicity,[18] and these SOC types can be induced by the noncoplanar arrangement of chiral organic ligands, ensuring that only one spin-channel is dominant for transport and luminescence.[19] In addition to OSCs and OIHPs, 2DMs consist of materials with excellent spin transport and broadly distributed SOC strength for effective spin manipulation.[10a, 20] Besides the unique intrinsic SOC characteristics, these emerging spintronic materials also have chiral-induced spin selectivity (CISS) [18a, 18e, 18f, 21] and electrical and optical properties,[3a, 3b, 22] which are essential for exploiting spin-related multifunctionalities (more details in Section 5). Typically, CISS describes the selective transport of electrons with different spin states, according to the chirality. These intriguing materials and multifunctionalities have already enriched experimental and theoretical research in the field of spintronics and will certainly play a critical role in inspiring next-generation spin-memories and computing devices.

In this review, we discuss the recent developments in spintronics based on OSCs, OIHPs, and 2DMs and summarize the specific material requirements for different spin-dependent applications. We first introduce spin transport and spin manipulation characteristics for each class of materials, according to their intrinsic chemical compositions and structures. Then, we

discuss the multipurpose applications of these materials by integrating their spintronic properties with chiral-induced spin selectivity (CISS), electrical and optical properties. Finally, we overview the challenges, opportunities, and research directions of each emerging spintronic materials and also propose integration between different materials and functionalities.

2. Organic Semiconductors (OSCs)

OSCs are mainly composed of light elements, such as H, C, N, and O; therefore, they possess weak intrinsic SOC and can maintain the spin coherence state for a long time, even at room temperature (RT).[23] Due to the long spin lifetime of the order of milliseconds or even seconds,[24] OSCs can serve as potential spin transport materials.[5i, 25] Combining spin transport properties with easy chemical tailoring, abundant photoelectric properties,[26] and the flexibility of OSCs,[27] significant achievements have been made in terms of mechanism investigation and multipurpose applications.

2.1. Spin Transport

In OSCs, the spin lifetime will be mainly influenced by the spin relaxation factors of SOC and HFI.[11e, 11g, 12-13, 28] SOC consists of the interaction between electron spin and orbital angular momentum, whose strength will be strongly affected by the atomic number of elements and chemical structure. Since SOC strength is proportional to the fourth power of the atomic number, heavy atoms should be avoided in the molecular design of OSCs. Some studies demonstrated that the SOC significantly decreased with the use of light elements in OSCs.[28d, 29] The correlation between molecular geometry and SOC strength has attracted significant attention. Due to the orthogonal arrangement of the three ligands in tris-(8-hydroxyquinoline) aluminum (Alq_3), it was found that Alq_3 had a larger SOC strength than sexithienyl (T6) and copper phthalocyanine (CuPc), even though the atomic weight of Al in Alq_3 was smaller than that of S in T6 and that of Cu in CuPc.[11g, 28b] Furthermore, the curvature degree of conjugated structures was also demonstrated to have a large impact on SOC strength. For spherical molecules C_{60} and C_{70}, the experimental results showed that the larger curvature degree of C_{60} than the C_{70} molecules directly led to a larger spin relaxation strength and thus a lower spin diffusion length in the C_{60} molecules, even though the mobility of C_{70} was lower than that of C_{60} (**Figure 1**a-i, ii).[30] However, for straight chain molecules, studies found that the curve-structure molecule (C-C12-DTBTBT) corresponded to a lower SOC strength compared to the linear geometry molecule (L-C12-DTBTBT), and the SOC strength of C-C12-DTBTBT with sulfur was even comparable to that of pure hydrocarbons.[29a] These results revealed the

important influence of spin density distribution, i.e., the molecular-geometry-induced spin density distribution could suppress the SOC originating from heavy atoms. The above reports suggest that the in-plane curvature of the conjugate plane in the molecule tends to increase the SOC strength. The topological phases in the C_{60} and C_{70} molecules also induced a charge hopping between the orbitals in the π and σ bands between the neighboring carbon atoms, resulting in so-called curvature SOC. Along the out-of-plane direction, spin density distribution should be considered. Spin density distribution resulting from the molecular geometry can almost completely suppress the SOC induced by heavier atoms. And such suppression is more significant in linear geometry molecules.

In another intrinsic spin relaxation effect, the HFI originates from the half-integer nuclear spins of atoms (i.e., ^{1}H, ^{9}F, ^{27}Al, ^{63}Cu).[28j] The half-integer nuclear spins can generate an effective magnetic field, which will interact with the electrons and result in spin relaxation.[28e, 28j] Isotope substitution was found to be an effective method for reducing HFI. Nguyen et al. studied the isotope exchange effect on spin responses in OSVs based on the π-conjugated polymer poly(dioctyloxy)phenylenevinylene (DOO-PPV). By replacing all hydrogen atoms (H) with deuterium atoms (D), the spin relaxation process caused by HFI was significantly suppressed, resulting in an increase in both the spin diffusion length and magnetoresistance (MR) signal (Figure 1a-iii, iv).[28g, 28j]

In addition to improving τ_s, improving mobility (μ) was also found to be critical for enhancing spin transport since the hopping-related spin diffusion constant is proportional to μ, according to

$$D_{hop} = \mu k_B T / e, \quad (4)$$

where k_B is the Boltzmann constant, T is the temperature, and e is the elementary charge. Mainstream OSCs used in spintronics have relatively low μ values, with typical values of around the magnitude of 10^{-7} to 10^{-4},[5h, 8a, 8f, 31] which significantly decreases the magnitude of λ_s. This is also the main reason for the relatively low spin diffusion length of OSCs compared to other spintronic materials. Accordingly, OSCs with high mobility may be used to achieve a long spin diffusion length. The N-type semiconducting polymer P(NDI2OD-T2) with electron mobility up to 0.20–0.85 $cm^2 \cdot V^{-1} \cdot s^{-1}$ was successfully used as a spin transport material, and a spin diffusion length of 41.87 nm at RT was achieved due to the high short-range order and face-on molecular packing of P(NDI2OD-T2).[32] Single-crystal OSCs with a pure composition and long-range ordered structure could potentially exhibit high field-effect mobility and spin lifetime and are likely to achieve ultra-long λ_s.[33] For example, Tsurumi et al. reported on a type

of OSC single crystal with μ = 13 $cm^2 \cdot V^{-1} \cdot s^{-1}$ and τ_s = 470 ns. The coexistence of an ultra-long spin lifetime and band-like charge transport resulted in a micrometer-scale λ_s.[34] However, constructing single-crystal-based spintronic devices without damaging the properties of single crystals remains a significant challenge.

From the aspect of spin transport regimes, the spintronic performance in materials and devices such as the diffusion length etc. is closely related to the mechanism of spin transport.[35] In pure single-component OSCs, spin theoretically transports via the LUMO or HOMO level, and it is generally considered a hopping-dominant spin transport regime (as shown in Figure 1b-i).[5h, 8h, 15a, 36] However, in real experiments, interfacial penetration usually results in a damaged interface and induces tunneling spin transport in OSCs.[8a] To decrease the influence of damaged interfaces during device preparation, Hueso et al. developed a low-temperature and rate-control evaporation technology, inducing a hopping spin transport regime and achieving a long spin transport distance of 180 nm.[15a, 15b, 36] Moreover, Hu et al. developed a mechanically transferrable top electrode method to achieve a damage-free interface, which provided a progressive strategy for improving interfacial quality.[37] From the other view, with high-density impurities in OSCs induced by metallic atoms or oxygen molecules, an impurity band will form in the gap between the HOMO and LUMO levels of OSCs. A high impurity density can lead to strong wave-function overlapping, and as this increases, the dominant spin motion will gradually transform from hopping to exchange coupling, which is much faster than hopping transport.[35a, 38] This exchange coupling spin transport can also be achieved by spin pumping injection from FM into the doped OSCs whose carrier concentration should be more than 10^{18} cm^{-3}.[35, 39] Therefore, in OSCs with concomitant hopping and exchange coupling spin-transport regime, the spin diffusion constant can be expressed as follows:

$$D = D_{hop} + D_{exc}, \tag{5}$$

where D_{exc} is the exchange-dominant coupling constant, given by

$$D_{exc} = 1.6J(R)R^2/\hbar, \tag{6}$$

where $J(R)$ is the exchange interaction and is closely related to the distance between carriers.[35a] Accordingly, the spin transport regime, as well as D_{hop} + D_{exc}, can be modulated along with changing the carrier concentration, as shown in Figure 1b-iii. A summary of the spin transport performance of commonly used OSCs is shown in **Table 1**. To the best of our knowledge, the current longest spin diffusion length exceeds 1 μm at RT,[35a] which is achieved in device with exchange coupling transport regime; this result is comparable to some well-known long-spin-diffusion-length materials, such as graphene.

Table 1. Summary of organic semiconductors (OSCs) and their typical spin-related parameters. Note: the parameters of the same material may have some differences, due to the variations in fabrication conditions and device structures.

Material	Mobility (μ) [$cm^2 \cdot V^{-1} \cdot s^{-1}$]	Spin lifetime (τ_s) [ns]	Spin transport distance (λ_s) [nm]	Magnetoresistance (MR)
Alq_3[8a]	2.5×10^{-5} (n)	—	40 at 11 K	40% at 11 K
Alq_3[24a]	2.5×10^{-5} (n)	1×10^9 at 1.9 K	~4 at 50 K	—
Alq_3[40]	—	—	—	~550% at 10 K
C_{60}[5h]	1.4×10^{-5} (n)	—	110 at RT	5.3% at RT
C_{60}[30]	1.4×10^{-5} (n)	—	86 ± 8 at 120 K	−13.3% at 20 K
C_{70}[30]	—	—	123 ± 13 at 120 K	−9% at 20 K
H-DOO-PPV[28g]	—	—	16 at 10 K	2% at 10 K
D-DOO-PPV[28g]	—	—	49 at 10 K	45% at 10 K
$F_{16}CuPc$[15a]	9×10^{-4} (n)	—	180 at RT	4% at RT
P(NDI2OD-T2)[32]	0.20–0.85 (n)	—	41.87 at RT	6.8% at RT
C_{10}-DNBDT-NW single crystal[34]	13	470 at 50 K	1.6×10^3 at 50 K	—
PBTTT[24b]	~ 3×10^{-5}	2×10^7 at 200 K	200 ± 30 at RT	—
F4TCNQ-doped PBTTT[35a]	~ 4	22	1.2×10^3 at RT	—

2.2. Spin manipulation

Spin manipulation generally means the capability to control the spin orientation of a single electron, with a strong SOC commonly considered a fundamental condition. Thus, spin manipulation is difficult to achieve in OSCs due to their intrinsically weak SOC strength, which has been widely verified and reflected in the difficult-to-measure Hanle effect.[41] Many studies have attempted to explore this issue. Through spin pumping injection and exchange coupling spin transport, Watanabe et al. made a major breakthrough in measuring the Hanle effect in OSCs, demonstrating that spin transport could occur in PBTTT molecules.[24b] However, Yu once proposed that the exchange coupling spin transport mode in OSCs would suppress the Hanle effect,[35b] which was also demonstrated by Jiang et al.[39] Afterward, Yang et al. observed the Hanle effect in an Alq_3-based spin valve at 10 K under a 7 T magnetic field, providing the

first evidence of the Hanle effect achieved by electrical spin injection in OSCs (Figure 1c). These innovative results were attributed to a large MR of up to 440%, along with effective spin injection by substituting the LSMO electrode with $(La_{2/3}Pr_{1/3})_{5/8}Ca_{3/8}MnO_3$ (LPCMO).[40] It should be noted that it is exchange-coupling dominated spin transport in this device. To date, only very few relevant studies[24b, 40] reported the observation of Hanle effect in OSCs. For the device featured by exchange coupling spin transport regime, whether Hanle effect can be detected is still controversial and further investigation is needed to solve this problem. To realize spin manipulation in OSCs, relevant studies have been conducted despite the challenges, and the next major breakthrough in the organic spintronic field may be in the research direction of exploring the spin manipulation characteristics of OSCs.

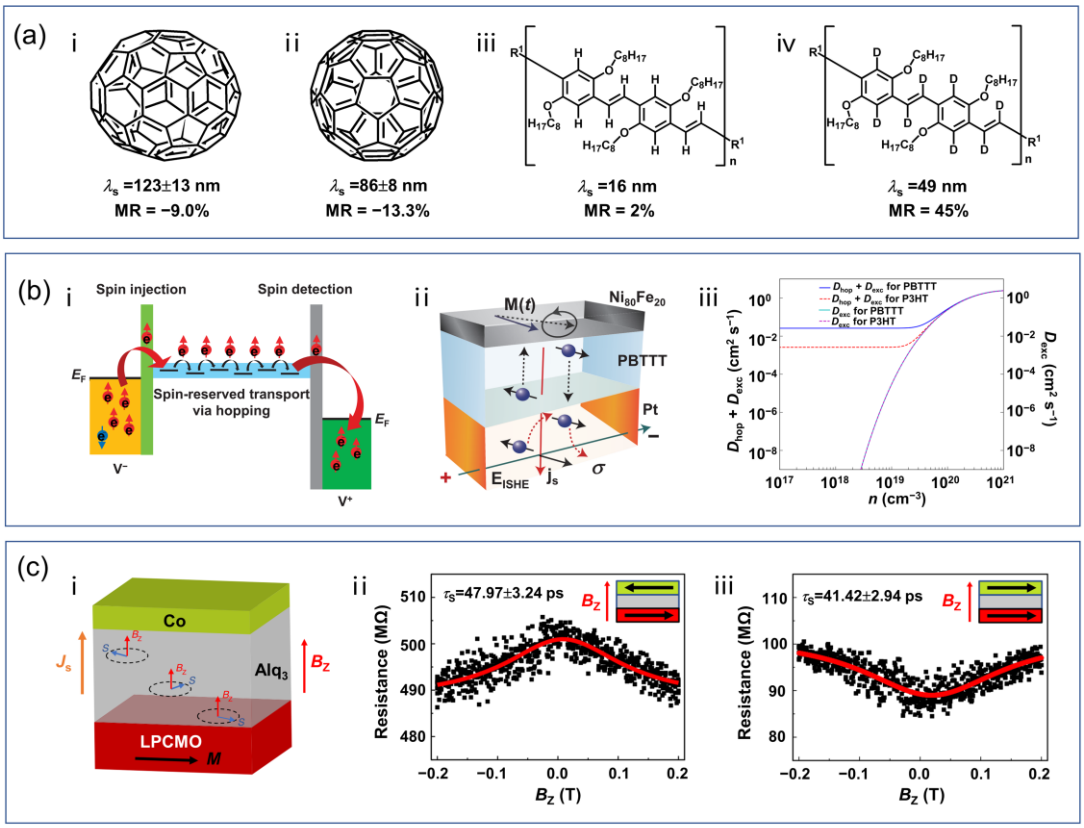

Figure 1. a) Molecular structures of (i) C_{70}, (ii) C_{60}, (iii, iv) H− and D−poly(dioctyloxy)phenylenevinylene (DOO-PPV), where H− and D− indicate protonated (^{1}H) and deuterated hydrogen (^{2}H), respectively. b) Schematic diagrams of spin transport regimes, (i) hopping, (ii) exchange coupling, and (iii) their correlations with carrier concentration in organic semiconductors (OSCs). Reproduced with permission.[5h, 24b, 35a] Copyright 2013, 2014, Springer Nature. Copyright 2019, The Authors, published by Springer Nature. c) Hanle effect in an OSCs-based spin valve, (i) schematic illustration of the Hanle

effect in the spin valve structure by $(La_{2/3}Pr_{1/3})_{5/8}Ca_{3/8}MnO_3$ (LPCMO)/Alq_3/Co; electrical Hanle effect when a perpendicular magnetic field (B_z) was applied to the device in the (ii) antiparallel and (iii) parallel magnetic configurations. Reproduced with permission.[40] Copyright 2019, The Authors, published by Springer Nature.

3. Organic-inorganic hybrid perovskites (OIHPs)

Multifunctional OIHPs have received significant attention and have been intensively studied for potential applications, mainly in highly efficient solar cells (SCs),[42] high brightness and color-purity light emitting diodes (LEDs),[43] and extremely sensitive photodetectors (PDs).[44] Low temperature and solution-processable properties can further broaden their applications in future flexible, wearable, and semitransparent electronics.[45] In general, OIHPs can be categorized according to three-dimensional (3D), two-dimensional (2D), and quasi-2D configurations.[22a, 46] All 3D OIHPs have a common chemical formula such as ABX_3, where A, B, and X represent an organic cation (methyl-ammonium (MA), formamidinium (FA)), a metal cation (Pb, Sn, Ge), and a halogen anion (Br, I, Cl), respectively. 2D configurations can be made more complex by introducing additional organic large-sized cations. An initial tetragonal structure can be energetically stabilized by phase transition toward a layered structure with a generic formula $A'A_{(n-1)}B_nX_{(3n+1)}$ after thermal treatment. The number of perovskite interlayers will actually determine certain material dimensionalities, such as n = 1, 2, 3, and 4. In addition, OIHP-based nanomaterials, such as nanowires, nanopalletes, and quantum dots, have also shown extraordinary optoelectronic properties in lasing and light emitting applications.[47] In principle, the electronic structures of OIHPs will be primarily determined by the inorganic crystalline frameworks.[48] The frameworks can be embedded with randomly oriented and caged organic chemical constituents. Occasionally, the structures may simultaneously offer semiconducting, ferroelectric, and spin-related characteristics.[3s, 9d, 49] A prototypical OIHP, such as $MAPbI_3$, usually undergoes phase transitions among the cubic, tetragonal, and orthorhombic crystals at different temperature intervals. The Pb and I of the inorganic framework PbI_3^- can offer relatively large SOC strengths at the conduction bands, eventually contributing to non-degenerated energy level splitting.[50] Of note, conventional semiconductors such as Si and GaAs have stronger SOC manifestations in valence bands, with the conduction band minimum and valence band maximum states primarily constructed by the Pb-6*p* and I-5*p* orbitals.[51] However, MA^+ will have little impact on band-edge states, with its organic characteristic showing minimal dispersion. Theoretically, the presence of stronger SOC will accelerate hot electron and hole relaxations while allowing efficient intersystem crossing

to long-lived triplet states,[52] thus assisting in elongating the charge carrier lifetime. However, SOC may cause spin de-phase in spin transport. Nevertheless, the high carrier concentrations and mobility of $MAPbI_3$ may make spin injection more efficient by electrical means via ferromagnets, and even avert the conductivity mismatch of ferromagnets and hybrid perovskites.[53] Despite this, $MAPbI_3$ was shown to have a remarkable Rashba effect due to a lack of structural inversion symmetry,[51b, 54] resulting in spin-dependent degenerated band splitting, even without external magnetic fields. This effect was predicted to suppress effective masses for electron and hole carriers, and as a result, they may acquire higher speeds. A summary of the optical gap energy variations with and without the impacts of SOC and the Rashba effect for $MAPbI_3$ of different crystalline phases was provided by S. McKechnie et al.[55] In-depth explorations of the spin-related phenomena in various types of OIHPs remain to be conducted, to fully release the multifunctional properties of OIHPs.

3.1. Spin transport

Although OIHP-based high-performance photovoltaics and light-emitting devices have achieved significant progress over the past decade, unfortunately, only a few reports are available regarding spin-polarized electronic transport and spin manipulation for hybrid perovskite systems. A summary of the reported spin transport performance of OIHPs is presented in **Table 2**. In 2019, Wang et al. demonstrated a green color spin LED fabricated using ferromagnet oxide LSMO and $MAPbBr_3$.[56] In addition, MR-based vertical spin valves such as LSMO/$MAPbBr_3$/Co/Au were studied in the same work. Both the optical and electrical Hanle measurements were carried out experimentally, and the researchers claimed that the exciton and electron spin lifetimes were measured at about 491 ± 17 ps and 936 ± 23 ps, respectively. In this case, the magnetic field was available for spin manipulation and detection. Moreover, a parallel work was conducted by studying various OIHPs with different organic cations and halogen ions (i.e., $MAPbBr_3$, $MAPbI_3$, and $FAPbBr_3$).[9b] Among these three, $MAPbBr_3$ produced the largest MR and the longest spin lifetime of approximately 802 ± 32 ps (**Figure 2**a), and $FAPbBr_3$ generated the longest spin diffusion length of approximately 206 ± 12 nm.[9a] A surprisingly long spin lifetime of more than 1 ns at 4 K was observed by Odenthal et al. for $CH_3NH_3PbCl_xI_{3-x}$ using the time-resolved Faraday rotation technique.[57] It was also speculated that the Rashba effect could slow down charge-carrier recombination, although SOC remained strong.[58] Nevertheless, the underlying mechanism is still under debate. In 2019, Wang et al. also studied spin-polarized electronic transport through a $MAPbI_{3-x}Cl_x$ based spin valve at RT.[5g] The results showed that the magnetic coercive fields of MR were highly

dependent on ferromagnet and $MAPbI_{3-x}Cl_x$ spinterfaces, indicating that the spin-dependent interfacial density of states (DOS) and electronic structures were decisive for the generation of MR. Despite this, spin accumulation at hybrid interfaces has been carefully studied via field-dependent capacitance-frequency spectroscopy. Since OIHPs are photoactive, the light-enhanced spin transport was studied in a $MAPbI_3$-based spin valve.[59] A large spin diffusion length of approximately 81 nm at 10 K was reported for a polycrystalline film, and the diffusion length could be further extended up to about 1 μm using a single crystal. In addition to these, the spin transport properties of $MAPbI_{3-x}Cl_x$ were extensively studied by the spin-pumping induced inverse spin hall effect (ISHE),[60] and the spin diffusion length was about 61 ± 7 nm. The spin lifetime of a NiFe/$MAPbBr_3$ structure was also studied by the spin pumping method. The lifetime was found to be approximately 189 ps at RT. The structure may offer a significant enhancement of the spin lifetime due to the formation of interfacial Rashba states.[61] Another intriguing study of spin transport involved spin Seebeck thermopower (SSTP) in an $MAPbBr_3$-based nonlocal structure.[62] An effective magnon injection was realized through an NiFe ferromagnet. With appropriate doping by Cr, both increases of the magnetic moment density and in-plane inverse Rashba-Edelstein effect synergistically led to SSTP enhancement.

Apart from spin injection and spin-polarized electronic transport through the ferromagnets for OIHPs, other relevant carrier transports without involving ferromagnets include magneto-photocurrent and magneto-electroluminescence-based magnetic field effects (MFEs). In 2015, Zhang et al. carried out a systematic study of MFEs in an $MAPbI_{3-x}Cl_x$ system.[63] The researchers demonstrated pronounced magneto-photocurrent and magneto-electroluminescence, and the underlying principle was attributed to the Δg (i.e., of approximately 0.65 in the study) mechanism, in which the relative difference of the *g*-factor for the photo- and electrically generated electron-hole pairs determined the occupations of the spin singlet and triplet states (Figure 2b). Also, in 2015, a parallel work focusing on MFEs in an $MAPbI_{3-x}Cl_x$ system was conducted by Hsiao et al.,[64] where pronounced magneto-photocurrent with a positive sign was produced when the illumination intensity exceeded a certain threshold. The researchers speculated that an applied magnetic field could suppress spin mixing at photoexcited states, consequently leading to a decrease in the electron-hole triplets but to an increase in its singlets. This work may offer a method for increasing the photocurrent by adjusting the spin statistics. Zhang et al. further extended this work by considering the replacement of metal element Pb by Sn to reduce the SOC strength and to suppress the conversion from photogenerated singlets to triplets.[65] Because of the decrease in the triplets in $MASnI_3$, it produced less photocurrent. Banerjee et al.[66] also studied spin mixing for various

OIHPs, including $MAPbI_3$, $MAPbBr_3$, $MAPbCl_3$, and $FAPbI_3$, by comparing perovskites composed of different organic cations, where $FAPbI_3$ with a pseudocubic structure exhibited enhanced SOC compared to octahedral titled tetragonal structures, such as $MAPbI_3$. Among the three halogen elements (i.e., I, Br, and Cl), those composed of I exhibited a relatively stronger SOC. The magneto-photocurrent can also be measured in a typical sandwiched spin valve structure. Pan et al. performed a systematic study on magnetic and nonmagnetic interfaces for 3D and quasi-2D OIHPs, such as $MAPbI_{3-x}Cl_x$ and $(PEA)_2(MA)_3Pb_4I_{13}$.[67] The study found that the spin valve structure could significantly enhance the magneto-photocurrent effect, and it showed remarkable responses to left- and right-circularly polarized light. This enhancement was possibly due to the formation of ferromagnet-perovskite spinterfaces.

Table 2. Summary of organic-inorganic hybrid perovskites (OIHPs) and their typical spin-related parameters. Note: the parameters of the same material may have some differences, due to variations in fabrication conditions and device structures.

Material	Mobility (μ) [$cm^2 \cdot V^{-1} \cdot s^{-1}$]	Spin lifetime (τ_s) [ns]	Spin transport distance (λ_s) [nm]	Magnetoresistance (MR)
$MAPbBr_3$[9b]	—	0.802 ± 0.032 at 10 K	221 ± 18 at 10 K	25% at 10 K
$MAPbI_3$[9b]	—	0.356 ± 0.022 at 10 K	108 ± 11 at 10 K	5% at 10 K
$FAPbBr_3$[9b]	—	0.788 ± 0.026 at 10 K	231 ± 12 at 10 K	16% at 10 K
$CH_3NH_3PbCl_{3-x}I_x$[60]	0.98 (n) & 1.32 (p)	1.5 ± 0.3 (n) & 1.1 ± 0.2 (p) at RT	61 ± 7 at RT	0.57% at 10 K
$MAPbI_3$ thin films under illumination[59]	0.53 @ RT	—	81 at 10 K	97% at 10 K
$MAPbBr_3$ single crystals[59]	48 @ RT	110 at 10 K	1×10^3 at 10 K	11.2% at 10 K
NiFe/$MAPbBr_3$ single crystals[61]	—	0.189 at RT	—	—

3.2. Spin manipulation

As previously mentioned, the strong SOC and remarkable Rashba effect were the preferred characteristics for spin manipulation in OIHPs. Focusing on SOC, Hu et al. initiated systematic studies from material and magneto-photocurrent aspects, which could be potentially applied as the basis for spin manipulation in perovskite systems. Experimentally, several methods have been used. (i) Various chemical constituents have been used for hybrid perovskite syntheses.

For example, by replacing Pb with Sn, an increase in photocurrent from 0.25% to 1.25% was achieved.[65] Furthermore, by tailoring the molar ratios of MA and FA with different dipole moments in Pb-halide perovskites,[68] the SOC strengths could be affected by analyzing the magneto-photocurrent line shapes, and researchers postulated that these were primarily due to the suppression of spin mixing. (ii) OIHPs can be rationally doped with organic or inorganic materials. For example, non-fullerene organic small molecules such as 3,9-bis(2-methylene-(3-(1,1-dicyanomethylene)-indanone))-5,5,11,11-tetrakis(4-hexylphenyl)-dithieno[2,3-d:2',3'-d']-s-indaceno[1,2-b:5,6-b'] dithiophene (ITIC) or transition metals such as manganese (Mn) were found to be functional enhancements of SOC.[69] Moreover, a large organic cation (i.e., PEA^+) was also used in 2D and 3D mixed Pb-Sn alloyed perovskites to improve SOC.[70] (iii) Externally applied mechanical strains may also influence SOC strength to a certain extent.[71] Thus, the method is of particular importance when assessing flexible OIHP-based electronics.

Despite SOC, the Rashba effect appears to be inherent for many OIHPs, and it is thought to be very useful for spin manipulation.[17a, 17c, 51b, 58b] Analogous to SOC, the Rashba field strengths are known to be material dependent and can be further adjusted through changing inorganic and organic compositions for the hybrid perovskites.[17d] This effect may serve as a critical route for spin manipulation based on spin precession in effective magnetic fields, and these effective fields can be induced by external electric fields due to the relativistic effect. The existence of this effect has been verified by many theoretical and experimental evidence.[17d, 54, 72] Typically, spin pumping, ultrafast spintronic terahertz emission, and circularly photogalvanic effect methods have been successfully applied to OIHPs and their devices to study the Rashba effect.[61, 73] From the aspect of OIHP-based devices, coherent spin transport lengths of the devices need to be reached to effectively achieve spin manipulation. Moreover, external gate voltages must be functional for effective manipulation of spin precession in the transport channels. For example, Rashba band-based electrical transport has been realized by spin-photogalvanic phenomena.[74] These phenomena stem from circularly and linearly polarized light-generated electrical currents, with different magnitudes of the photocurrents due to the presence of spin-dependent degenerated energy sub-bands in momentum vector spaces. These phenomena have also been observed in chiral OIHPs.[75] Since some OIHPs can exhibit ferroelectric properties,[76] in which externally applied electric fields along certain crystallographic axes can generate ferroelectric bulk polarization, these properties can be further used to control the inversion symmetry breaking field. When electric fields are applied in opposite directions, the ferroelectric polarizations can be coupled with spin splitting, and the spin textures will be reversible through ferroelectric switching. As a result, two distinct

ferroelectric Rashba bands with contrasting orbital and spin characteristic can be realized.[77] Therefore, the development of ferroelectric Rashba perovskites is promising for the switchable Rashba effect and spin manipulation.

From the above discussion, electrical spin transport and spin manipulation in OIHP-based spintronic devices remain at an early stage, and preliminary work should focus on device fabrication and optimization methods, involving high crystalline quality and solution-processable OIHPs. Some newly developed fabrication methods in photovoltaics may also be utilized, such as annealing-free and co-evaporation techniques. In addition, to develop OIHP-based spin valves with large MR, small switching fields and fast switching speeds are of particular importance to systematically study material- and interfacial-dependent magneto-transport. Currently, most studies have focused on magneto-photocurrent in OIHP-based photovoltaics. Although the Rashba effect is an innate characteristic of OIHPs, the effective use of Rashba bands for spin manipulation via electrical means has yet to be presented, with relevant studies still focusing on the photo-galvanic effect using the optical method. Finally, concrete spin transport and spin manipulation theories should stay up-to-date with newly developed experimental results for these types of hybrid materials.

Current studies on regulating the strength of the Rashba effect have established a foundation for future spin manipulation investigations. For example, the number of inorganic layers (n) between two organic parts in layer-by-layer OIHP structures was closely correlated to Rashba band splitting in 2D OIHPs, where intrinsic Rashba splitting only occurred when n was even (n = 2) rather than when n was odd (n = 1 and n = 3) (Figure 2c).[58a] Moreover, it was found that electron spin can be controlled by electrically optimizing the Rashba effect in OIHPs with ferroelectricity.[78] Based on ferroelectric OIHPs, a new generation of non-volatile spin memory devices may be realized by electrically modulating spin polarization. Specifically, OIHPs possess great potential in spin manipulation research, and significant achievements are expected in the future, including problem solving and opportunity exploration in OIHP-based spintronics.

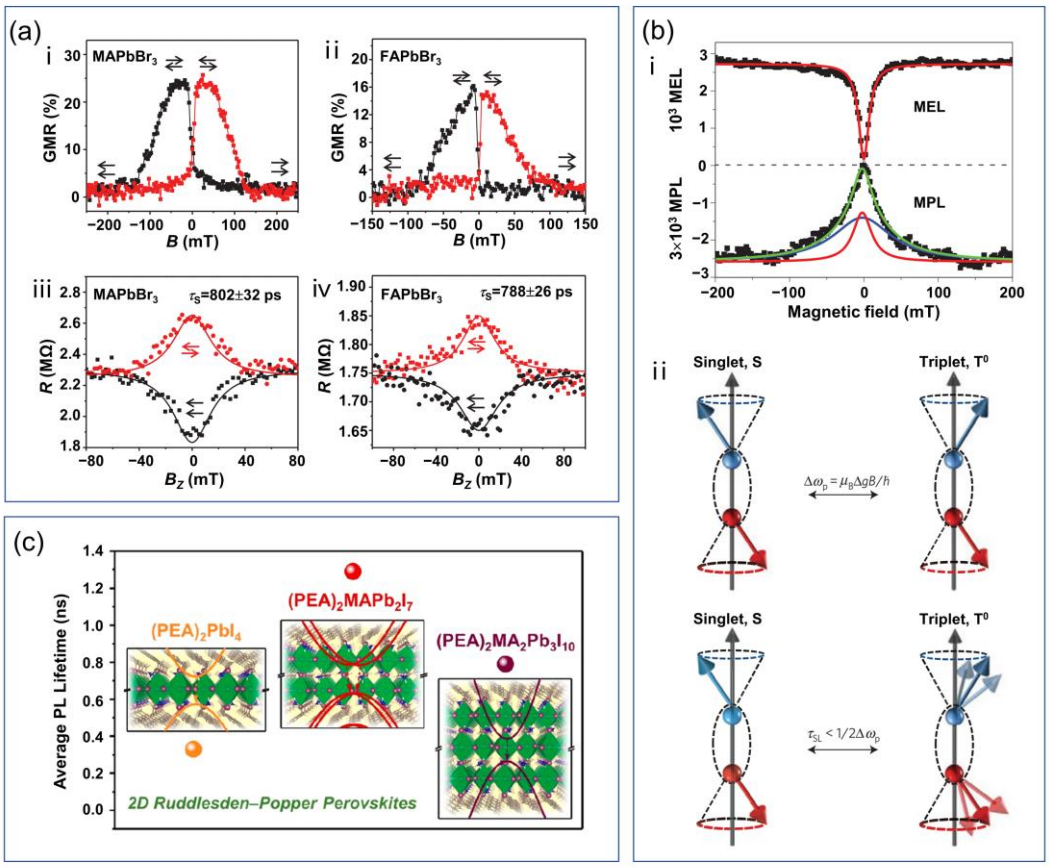

Figure 2. a) MR and Hanle effect measurements in spin valves based on organic-inorganic hybrid perovskites (OIHPs) at 10 K. Giant magnetoresistance (GMR) response of spin valve based on (i) $MAPbBr_3$ and (ii) $FAPbBr_3$. Hanle response curves measured in (iii) $MAPbBr_3$ and (iv) $FAPbBr_3$-based spin valves, where the spin lifetimes of each OIHPs could be extracted by fitting the Hanle effect curves. Reproduced with permission.[9b] Copyright 2019, Wiley-VCH. b) (i) Magnetic field effect (MFE) in a $CH_3NH_3PbI_{3-x}Cl_x$−based device characterized by magnetoelectroluminescence (MEL) and magnetophotoluminescence (MPL) response; (ii) schematic diagram of the Δg spin-mixing mechanism to illustrate the MFE in OIHP, where MFE will diminish when the spin relaxation rate was much larger than the intersystem crossing rate between a spin singlet and triplet. Reproduced with permission.[63] Copyright 2015, Springer Nature. c) Layer-dependent Rashba band splitting in 2D OIHPs and its influence on the PL lifetime, where n is the number of inorganic layers in the OIHP structures. Reproduced with permission.[58a] Copyright 2018, American Chemical Society, https://pubs.acs.org/doi/10.1021/acs.chemmater.8b03436.

4. Two-dimensional materials (2DMs)

Two-dimensional van der Waals (vdW) materials that can be thinned to atomic thicknesses possess many exceptional physical properties favorable to the research and application on spin-related phenomena in classical and quantum devices. These include high mobility and weak SOC in graphene,[10a, 79] variable and tunable SOC in other 2DMs, unique spin-valley coupling in transition metal di-chalcogenides (TMDCs),[80] and the spin-momentum locking in topological insulators.[3c, 10c, 81] These materials demonstrated an ultra-long spin transport distance and a superior spin manipulation ability, making them ideal candidates for fabricating proof-of-concept spintronic devices.[10a, 20b, 82] Heterostructural 2D spintronic devices can not only harvest the properties of each individual constituent layer, but can also demonstrate new physical properties due to reduced physical dimension, a unique band structure (pseudospin, spin-valley coupling) and the proximity effect (eg. Rashba-Edelstein effect). Their spintronic properties in combination with excellent optoelectronic and straintronic properties make 2DMs extremely attractive candidates for future research and applications in high-performance spintronic devices with novel functionalities.

4.1. Spin transport

Graphene as the pioneer and foremost material within the 2DMs family exhibits weak intrinsic SOC and HFI as well as high mobility, which are favorable for long spin lifetime and diffusion length. Theoretical calculations for graphene predicted a spin lifetime of more than 1 μs and spin diffusion lengths in excess of hundreds of microns.[83] However, the majority of the experimental reports using graphene spin valves, such as in **Figure 3**a, were still in the picosecond to a few nanosecond regime of spin lifetime, with a spin diffusion length of a few microns.[5b, 10a, 20b, 82, 84] Numerous efforts have been made to identify the source and nature of the spin relaxation processes, as Elliott-Yafet, D'yakonov-Perel, a mixture of both, or even Pseudospin-driven spin relaxation.[4b, 84c, 85] Experimentally, the discrepancies between experimental and theoretical studies, or among different experimental studies are considered to be related to different sources of spin relaxation, including scattering from impurities,[86] adatoms, ripples,[85b, 87] substrate,[85c] and spin absorption in ferromagnetic electrodes.[88]

Several attempts have been made to eliminate these negative impacts and to enhance spin-related performance. **Table 3** presents a summary of the spin transport performance of graphene and a few other 2DMs. Standard strategies include suspending graphene above substrates (Figure 3b),[5c, 89] encapsulating graphene with hexagonal BN (h-BN) (Figure 3c),[88c, 90] and decoupling from the substrate by growing graphene on SiC or reducing the conductivity mismatch by using resistive contacts.[5b, 84b] Suspending graphene was shown to enhance the

mobility of graphene by up to 10^5 $cm^2 \cdot V^{-1} \cdot s^{-1}$.[91] As a popular substitute for dielectric substrate or insulating barrier, h-BN, as an insulating 2D material, has a small lattice mismatch with graphene (1.7%), is free of dangling bonds or surface charge traps, and can be easily assembled with graphene to form 2D heterostructures.[85a, 92] In graphene devices with h-BN substrates, RT phonon scattering was weakened by almost an order of magnitude, while mobilities were an order of magnitude better than on SiO_2.[92] The spin diffusion length was also increased up to tens of microns.[85a, 90, 93] As fabrication techniques continuously improve, it is likely spin transport will enter the ballistic regime where new quantum transport model will need to be considered.[94]

Table 3. Summary of two-dimensional materials (2DMs) and their typical spin-related parameters. Note: the parameters of the same material may have some differences, due to the variations in fabrication conditions, device structures, and measurement techniques. Unless otherwise mentioned, tunnel barriers are typical oxide barriers such as Al_2O_3, Ti_2O_3, and MgO.

Material	Mobility (μ) [$cm^2 \cdot V^{-1} \cdot s^{-1}$]	Spin lifetime (τ_s) [ns]	Spin transport distance (λ_s) [μm]
Single graphene on SiO_2[84a]	2×10^3	0.155/0.177 at RT	1.6/2.0 at RT
Suspended graphene[90b]	2.1×10^4	12.6 at RT	30.5 at RT
Suspended graphene[95]	3×10^5	0.15	4.7 at RT
h-BN encapsulated bilayer graphene[90a]	9×10^3	4	0.6 to 90
h-BN encapsulated bilayer graphene[93]	2.3×10^4	2.9	24 at 4K
h-BN encapsulated single layer graphene[96]	1.5×10^4	2 at RT	12 at RT
Single-layer graphene on h-BN[85a]	4×10^4	0.39 at RT	20 at RT
Graphene with an h-BN tunnel barrier[88c]	3×10^3	0.46	1.4 at RT
Graphene with an h-BN tunnel barrier[97]	2.3×10^3	0.056	1.14 at RT
Graphene with an h-BN tunnel barrier[98]	5.4×10^4	0.016	0.73 at RT
Single-layer graphene on WS_2[99]	5×10^4	0.005 at RT	2 at RT
Epitaxial graphene on SiC[5b]	1.7×10^4	100	100 at 1.4 K
CVD graphene[100]	3×10^3	1.75 at RT	~5 at RT
Six monolayer-thick MoS_2[101]	~6	46	~0.235 at ~10 K
Black phosphorus[102]	~1.5×10^3	~4 at 2.4 K	~6 at 100 K

Another source of relaxation is the invasive contact between graphene and magnetic electrodes. As with all semiconductors, spin injection from ferromagnetic metal into the semiconducting spin transport channel must overcome the problem of conductivity mismatch.[53] This is basically a discrepancy in the resistance a spin would have experienced within one spin diffusion length of transport in the metallic contact and spin transport channels. Because graphene is a semimetal and is more resistive than metallic contact, its spin resistance will be much larger, leading to a rejection of the majority of spins back into the magnetic contact where they relax, resulting in a problem of spin injection. The presence of these contacts in proximity to the transport channel will also cause additional spin relaxation. Conventional tunnel barriers such as MgO,[84d, 103] Al_2O_3 (Figure 3b),[84a, 104] TiO_x,[105], SrO,[106] and h-BN (Figure 3c) have been used to enhance the spin injection efficiency and prevent unnecessary spin relaxation.[88c, 97-98, 107] By using these barriers, researchers could fine tune the contact resistance to an optimal condition to achieve large MR, but not necessarily a long spin lifetime or spin diffusion length, because the larger the interfacial resistance, the better it would preserve the spins already in the channel. However, a large MR would require a balance between efficient injection and minimal spin relaxation, and this balance means optimum resistance window for large MR typically falls within around a few tens of kiloohms. In addition to tuning the barrier resistance, magnetic electrodes with a higher spin polarization could also be used. Recently, 2D layered FM metals such as Fe_3GeTe_2 (FGT) and $Cr_2Ge_2Te_6$ (CGT) were discovered,[108] with FGT possessing good metallicity, large perpendicular magnetocrystalline structures, and a high Curie temperature of ~200 K.[109] This discovery allowed researchers to fabricate fully 2D spin valves that were purely based on van der Waals (vdW) materials (Figure 3d).[110] For example, Lin et al. fabricated vertical FGT/MoS_2/FGT spin valves, and the study revealed the Ohmic contact at the FGT/MoS_2 interfaces, and the maximum spin polarization was 12.3 % in FGT, which was higher than that in conventional devices where metallic magnetic electrodes were used.[110a] Another study on FGT/InSe/FGT vertical spin valves also reported an MR as large as 41%.[111] These studies demonstrated that the electrical injection of spins into various 2DMs was highly efficient, creating possibilities for the study of spintronic properties of an entirely new class of multifunctional materials. With these possibilities, the optical, electrical, and magnetic control of spin transport can now be envisioned using semiconducting, ferroelectric, and magnetic 2DMs as the spin transport medium. Fundamentally, electron spin can also be used as an additional probe to investigate the fundamental relationship between structural anisotropy, e.g., the intralayer chemical bonds and interlayer vdW forces in 2DMs and the

electronic/spintronic properties. This includes, for example, the anisotropic spin relaxation properties for spins parallel and perpendicular to the 2D plane.[112]

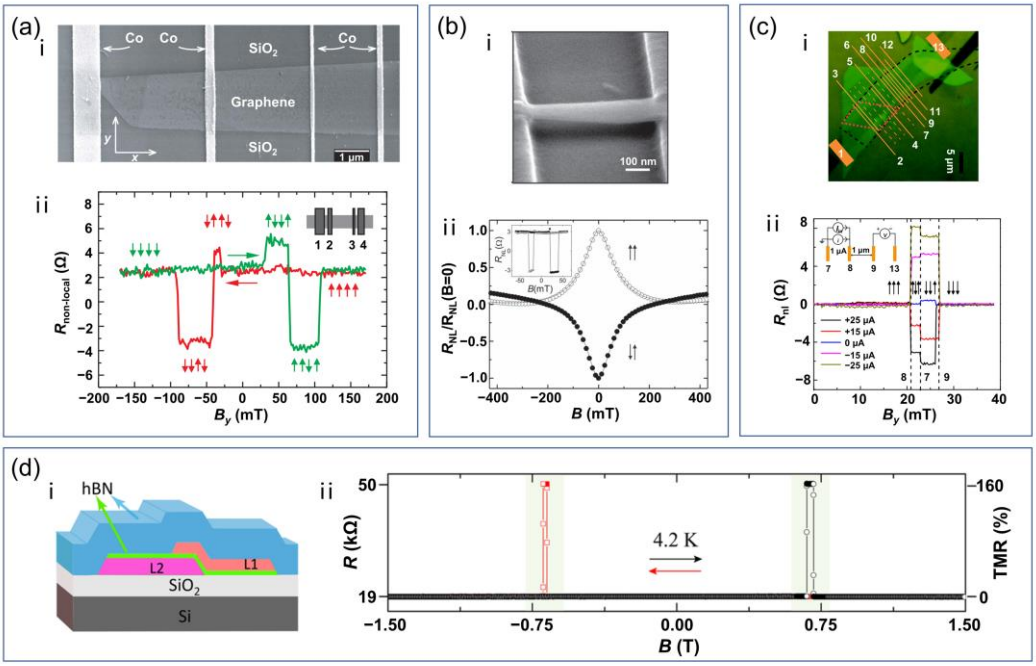

Figure 3. Spintronic devices based on graphene and 2DMs: a) normal graphene spin valves prepared on SiO_2 substrate, (i) SEM image of the device and (ii) nonlocal spin transport signal. Reproduced with permission.[84a] Copyright 2007, Springer Nature. b) Suspended graphene spin valves, (i) SEM image of the device and (ii) nonlocal spin transport signal including the Hanle measurement. Reproduced with permission.[89b] Copyright 2013, Wiley-VCH. c) Graphene spin valves with hBN tunnel barriers prepared on an hBN substrate, (i) optical image of the device and (ii) nonlocal spin transport signal. Reproduced with permission.[107] Copyright 2017, The Authors, published by Springer Nature. d) Fully two-dimensional spin valves using 2D magnetic electrodes and an hBN tunnel barrier, (i) schematic of the device and (ii) spin transport measurement. Reproduced with permission.[110b] Copyright 2018, American Chemical Society.

4.2. Spin manipulation

Along with preserving the pristine spintronic properties of graphene so that spins can be transported and manipulated over long distances and extended time, the properties of graphene may be enriched by doping or the proximity effect. This is achievable because the environment in and around where the spins are hosted will play a very important role in the overall spintronic properties of devices. Thus, precise control of the local environment has become the most versatile tool for building devices with conceptually new ideas and for studying the fascinating

physics down to the atomic scale. One important feature, for example, is the tunability of the SOC strength in graphene for the purpose of spin manipulation, as discussed below.

SOC is an important foundation for spin manipulation. This requirement means that although graphene is ideal for spin transport, it is not a good system for performing spin manipulation. To enhance the SOC strength of graphene, both the extrinsic sources of SOC and the spin-orbit proximity effect have been investigated. Adatoms, such as hydrogen atoms or Pb, have been used as an extrinsic source of SOC.[113] However, the addition of adatoms can result in disorder and scattering, giving rise to a trade-off between SOC and mobility. In addition, proximity-induced SOC in graphene by other functional materials holds the promise to harvest both its superior spin transport capability and realize spin manipulation. For example, the proximity effect in graphene on top of magnetic substrates or other 2DMs has been investigated both theoretically and experimentally.[98, 112, 114] Experimental measurements along this line include measuring the anomalous Hall effect and spin Hall effect in Hall bar-shaped graphene in a nonlocal geometry. However, assessing SOC using these approaches requires careful consideration of other spurious effects.[115] Another method of studying SOC in graphene involves monitoring the transport of spin current in graphene, which can be achieved by placing graphene spin valves in proximity to other 2DMs. By monitoring the spin current, the spintronic property of modified graphene can be inferred. These include enhanced SOC in graphene due to the proximity effect and spin-valley coupled phenomena (**Figure 4**a).[105a, 112, 114e, 116]

Compared to graphene, other 2DMs such as TMDCs have already shown a strong SOC effect and unique spin-valley coupling phenomena.[80b] Initial investigations of their spintronic properties have been hampered by the difficulty of electrically injecting electron spins. This technical difficulty has now been overcome and multiple research groups have successfully measured large MR with very sharp switching features in several 2DMs including MoS_2,[110a] WSe_2,[117] and InSe.[111] These findings may provide new opportunities for investigating the spin and valley degree of freedom and use them to develop new spin manipulation strategies.

Furthermore, the discovery of 2D ferroelectric (In_2Se_3, $CuInP_2S_6$),[118] magnetic (FGT), and multiferroic materials ($CuCrP_2S_6$)[119] and the demonstration of their electronic and/or spintronic devices form the necessary prerequisites for new spintronic devices that stretch beyond existing spin transistor proposals. Another unique property of 2D materials that has not been widely explored in spintronics is the fact that they can withstand very large strain, in the range of tens of percentage points, far beyond the limit achievable using conventional techniques in materials science.[120] This property has led to the observation of a range of phenomena related to strain, such as strain-controlled band gap, luminescence, and

magnetization.[121] This extra degree of freedom allows for the integration of straintronics into spintronics. Particularly attractive for fast and energy-efficient device operation are the significant advances achieved in the ultrafast phononic control of the physical properties of 2DMs using dynamical strain. Fast dynamic strain can be generated in 2DMs with frequencies reaching tens or even hundreds of gigahertz (Figure 4b).[122] The ability to integrate 2DMs with any arbitrary substrate is significantly advantageous in this regard, allowing for an extra degree of freedom to tune the frequency of dynamic strain, which in turn can be used to manipulate other physical properties, including spintronic properties.

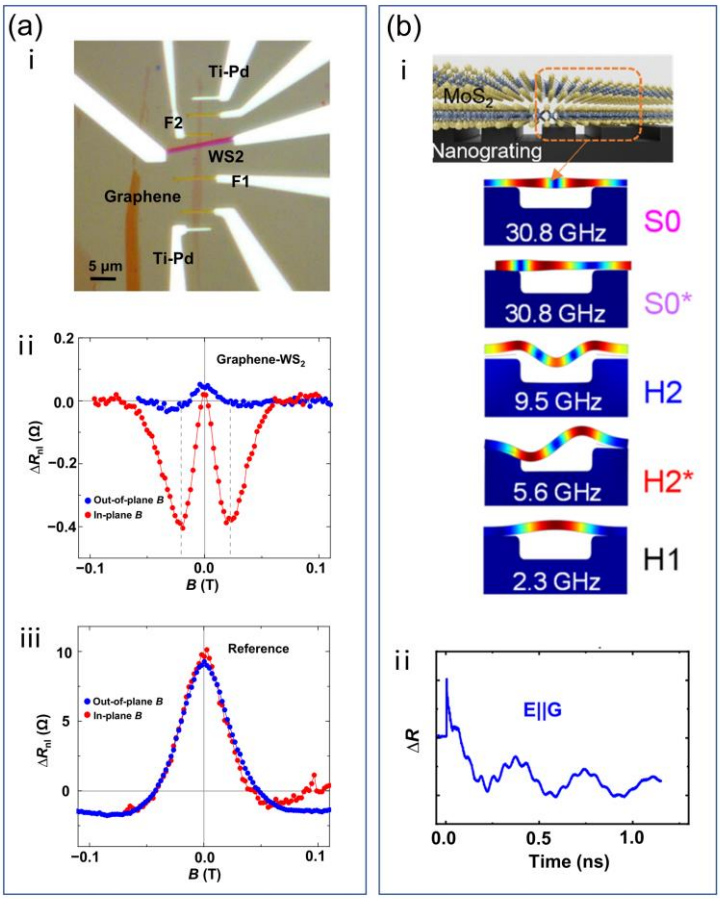

Figure 4. Tuning the properties of 2DMs: a) SOC of graphene tuned by the WSe_2-induced proximity effect at the interface: (i) optical image of the graphene spin valves, (ii, iii) Hanle measurement of the spin signal showing the asymmetric Hanle effect in graphene on top of WS_2. Reproduced with permission.[112] Copyright 2017, The Authors, published by Springer Nature. b) Ultrahigh-frequency strain control of the MoS_2 properties: (i) schematic of the 2D periodic phononic crystal with MoS_2 on top of nanograting and finite element simulation of the layer motion showing different phonon modes, (ii) temporal measurement of the measured reflectivity pump-probe signal showing high-frequency oscillations on top of a slow periodic

oscillating background. Reproduced under terms of the CC-BY license.[122f] Copyright 2022, The Authors, published by American Chemical Society.

5. Advanced Spintronics Concepts and Applications

With the current growth of promising spintronic materials, some advanced concepts and applications have been applied to efficiently and fully utilize the spin degree of freedom. This section reviews CISS for chiral materials, spin-photovoltaics, spin-LEDs, and spin transistors. With these, spins may be effectively manipulated from material geometries, such as helicity. Moreover, advanced spintronic applications should also meet the requirements of future electronic devices for energy savings.

5.1 Chiral-Induced Spin Selectivity

Chirality plays an exceptionally important role in broad disciplines including chemistry, biology, and physics. Chirality originates from the structurally symmetrical breaking of an object, where the chiral object does not overlap with itself after mirror reflection or inversion.[18a, 123] When massive spin particles are transported through a chiral material, a centripetal force will appear perpendicular to their velocity. The direction of the force parallel or antiparallel with respect to the velocity of the spin will depend on the handedness of the chiral material (i.e., either left or right handedness). Only a specific spin, with either a spin-up or spin-down polarized electron, will be favored, as shown in **Figure 5**a. This material-dependent transport behavior is termed CISS.[18e, 18f, 124] Essentially, spin can be coupled to the chiral material through chiral-induced spin orbit coupling. With this property, spin polarization and spin selective transport can be realized in the chiral material without the use of ferromagnets,[18e, 19d] and it may not require a large current density for changing magnetization, compared to spin transfer torque (STT).[125]

Theoretically, a complete understanding of CISS requires the consideration of a model for a particle transport throughout a helix. In fact, the helical structure can naturally assign an extra SOC for the particle. The Hamiltonian for the so-called geometric SOC (H_{ine}) in a helix can be written by:[18d]

$$H_{ine} = -\frac{\hbar\kappa}{4m} p\left(\boldsymbol{N}\times\boldsymbol{T}\right)\cdot\sigma, \tag{7}$$

where, $\hbar$ is the Dirac constant, κ denotes the helix curvature, m is the mass of the particle, p is the momentum, both $\boldsymbol{N}$ and $\boldsymbol{T}$ represent the normal and tangential vectors of the helix. σ is known as the Pauli spin matrices. It should be noted that the geometric SOC needs to be

distinguished from the atomistic SOC. It is independent on material constituents and is solely determined by the helical configuration. By considering an interlayer-based charge transport along a *z*-direction in 2D chiral perovskites, the conventional Hamiltonians for the dispersion function over the entire *k*-space can be extensively developed for an electron and hole by including the chiral-induced SOC such as:[18d]

$$H_e^{'} = \sum_k \left(\frac{\hbar^2 k_z^2}{2m_e} + \alpha_e \tau \sigma_z k_z \right), \tag{8}$$

$$H_h^{'} = \sum_k \left(\frac{\hbar^2 k_z^2}{2m_h} + \alpha_h \tau \sigma_z k_z \right), \tag{9}$$

where m_e and m_h are the effective masses for an electron and a hole respectively. α_e and α_h denote the corresponding effective SOC strengths due to chirality. τ represents material helicity ($\pm$ 1) and σ_z is the charrier spin ($\uparrow$ or $\downarrow$). Apparently, the extra SOC

$$H_{so} = \alpha_h \tau \sigma_z k_z, \tag{10}$$

changes sign when τ or σ_z is changed. In the case of an electrical field (ε_z) presents in the chiral perovskites, a nonzero magnetization (***M***) can be developed due to the geometric SOC and spin-dependent carrier distributions. The derivation for such macroscopic spin polarization, also known as the Edelstein effect, involves solving spin-dependent Boltzmann transport equations (f_k^z). The complete expression for ***M*** due to hole spin carriers can be written by:[18d]

$$\boldsymbol{M} = \sum_k f_k^z = \frac{e\hbar^2 \alpha_h \tau}{16 m_h \tilde{w}^{'} k_B T} \varepsilon_z N_0, \tag{11}$$

where *e* is known as the elementary charge, $\tilde{w}^{'}$ defines an acoustic phonon scattering even, k_B and *T* are the Boltzmann constant and the temperature respectively, N_0 represents the carrier density. By the observation of the above equation, the joint of a change of the material helicity and a non-equivalently chiral-induced carrier distribution gives rise to the generation of a nonzero spin-polarized macroscopic magnetization.

In this section, we mainly focus on newly developed chiral organic inorganic hybrid perovskites for advanced spintronic applications. Chiral perovskites consist of a group of 2D hybrid materials, in which chirality can be introduced by implanting chiral organic ligands into inorganic octahedral crystalline frameworks.[19b, 19e, 126] Over the past few years, many chiral hybrid perovskites have been successfully synthesized and optimized,[127] and despite spin transport, they can be used in magneto-optics,[10c, 128] nonlinear optics,[129] ferroelectricity,[130] and ferroelastic switches.[131] CISS can be mainly reflected from two aspects of spintronics,

with one consisting of spin transport by the electrical method, and the other based on the optical mean for circularly polarized luminescence (CPL).

From the aspect of spin transport and manipulation, one pioneering work focused on localized MR measurements for $(R\text{-}MBA)_2PbI_4$ and $(S\text{-}MBA)_2PbI_4$-based chiral lead halide perovskites using the magnetic conductive probe atomic force microscopic (mCP-AFM) technique (Figure 5b).[19c] The tricky part of the experiment was the utilization of a Co-Cr-coated tip, which could be pre-magnetized by a strong field prior to measurement. The chiral-dependent output currents with different magnitudes at a fixed bias voltage could be well detected for magnetization of the tip along two opposite directions (Figure 5c). Such transport behavior is equivalent to a single magnet-based tunnel junction due to existence of an air gap (i.e., FM/gap/chiral perovskite/metal). In principle, the tunneling current density (J_{tunnel}) can be described by:

$$J_{\text{tunnel}} \propto \int dE\left[f_{\text{F}}(E) - f_{\text{M}}(E)\right]|\text{T}|^2 n_{\text{F}}(E) n_{\text{M}}(E), \tag{12}$$

where $f_F(E)$ and $f_M(E)$ represent the Fermi-statistical distributions for the magnetic tip and the mental. $|T|^2$ represents the transmission probability across the chiral perovskite. Both $n_F(E)$ and $n_M(E)$ are the spin carrier densities for the magnetic tip and the metal respectively. Since the total current flux should contain both spin-up and spin-down polarized electrons, the manipulation of the magnetization for the magnetic tip will lead to the spin-dependent current density. Indeed, such current density has strong relationship with $\boldsymbol{M}$ in Equation (11).[18d] For example, if the tip is magnetized with a dominant spin-up polarization, the spin-dependent current fluxes could be written by:

$$J_{\uparrow(\downarrow)}^{Up} = \frac{1+(-)P}{2} J_0 \left(\frac{V}{V_0}\right)^2 e^{-\frac{V_0}{V}} \frac{1+(-)\bar{M}}{2}, \tag{13}$$

Conversely, when the tip is magnetized with a dominant spin-down polarization, the spin-dependent current fluxes could be written by:

$$J_{\uparrow(\downarrow)}^{Down} = \frac{1-(+)P}{2} J_0 \left(\frac{V}{V_0}\right)^2 e^{-\frac{V_0}{V}} \frac{1+(-)\bar{M}}{2}, \tag{14}$$

where P and V are the polarization and bias voltage respectively. Both J_0 and V_0 are the two factors determined by interfacial barrier heights and material thickness. $\bar{M}$ denotes electrical field dependent magnetizations. Despite this, clear hysteresis-like MR could be obtained from the layered structure, such as ITO/$(R\text{-}MBA)_2PbI_4$ (or $(S\text{-}MBA)_2PbI_4$)/NiFe/Au (Figure 5d). Because only one ferromagnet (i.e., NiFe) was used, the MR actually stemmed from the

magnetic coupling of the ferromagnet and chiral-induced magnetization. Recently, the spin-photogalvanic effect was demonstrated in the lateral devices of an Au/(R-MBA)$_2$PbI$_4$ (or (S-MBA)$_2$PbI$_4$)/Au configuration.[75b] The channel length was approximately 100 μm. With circularly and linear polarized photoexcitation, the light helicity-dependent short-circuit current exhibited decent two-fold symmetry for a full cycle in a broad temperature range (Figure 5e). The effect was possibly due to mutual interactions among the Rashba effect, CISS, and chiral-induced magnetization. The chiral-induced magnetization was also observed by the magneto-optical Kerr effect, previously observed for ((C$_8$H$_{11}$N)$_2$PbI$_4$)-based chiral perovskite.[10c] The Kerr signal at the chiral-OIHP/NiFe interface changed upon illumination and exhibited a linear dependence on the magnetic field, and these responses were chirality dependent. In addition, a recent study further extended the use of chiral perovskites in the field of spin caloritronics.[132] Spin currents produced by chiral phonons and thermal gradients could be realized in a 2D chiral perovskite system ((R-MePEA)$_2$PbI$_4$ and (S-MePEA)$_2$PbI$_4$), without involving any magnetic materials. Of note, the chiral-phonon-activated spin Seebeck (CPASS) effect should differ from the conventional CISS effect, with the chiral units acting as spin filters during electron transport. Instead, the CPASS effect may shed light on the high-efficient transduction of spin information in the absence of electron flow.

In contrast to spin transport, chiral perovskites have been intensively studied for CPL, with their natural optical activities (NOAs), such as circular dichroism (CD) and CPL, determined by CISS.[19d, 126b, 133] Upon photoexcitation, only one spin channel (i.e., spin-up or spin-down) will be dominant for absorption and emission. This characteristic was revealed in many newly synthesized chiral perovskites. In addition, recent studies also focused on the newly found chiral magneto-optical effect, including magneto-photoluminescence,[128, 134] in which the photo-induced fluorescent intensity and circular polarization could be manipulated by magnetic fields. This was theoretically studied due to the interplay between the perovskite exciton states and CISS.[18d]

Despite the chiral perovskites, chirality and CISS were also found in organics and 2D materials. According to the correlation of the chiral unit and the material framework, chiral materials can be divided into pure chiral molecules and composited chiral species (**Table 4**). Some chiral organic molecules have been reported, including double-stranded DNA,[135] helicenes,[136] and α-helix polyalanine,[125] usually in the forms of self-assembled monolayers (SAMs) and thin films. CISS will likely be relatively stronger for SAMs; for example, the spin polarization of double-stranded DNA can exceed 60%, even at RT. This could be enhanced with an increase in the DNA length.[135] Moreover, helical supramolecular nanofibers were

reported, resulting in more than 85% spin polarization at RT.[137] Other self-assembled super-helical conducting polymer microfibers could obtain spin polarization of 80%.[138] This was ascribed to multi-stage spin selectivity by long-range molecular ordering in the chiral building blocks. In addition, a new class of composite chiral species was developed by incorporating layered 2D atomic crystals with self-assembled chiral molecules. Spin polarization greater than 60% and an MR larger than 300% were achieved in their tunnel junctions. The robust properties of these chiral molecular intercalation superlattices make them extremely suitable for constructing stable solid-state devices.[139]

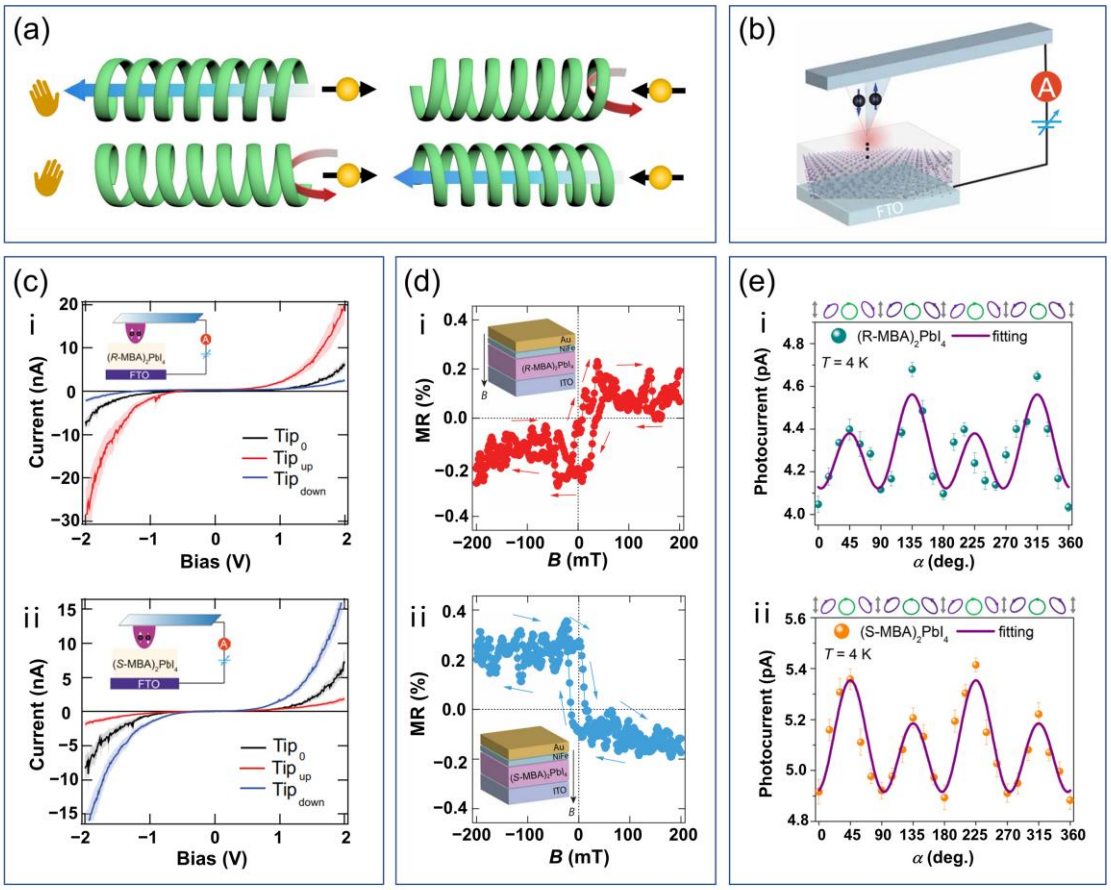

Figure 5. a) Schematic diagram of the origin of chiral-induced spin selectivity (CISS) effect: electronic charge distribution in chiral molecules results in a chiral electrical field, leading to a spin polarization effect. Reproduced with permission.[139] Copyright 2022, The Authors, published by Springer Nature. b) Schematic diagram of magnetic conductive probe atomic force microscopic (mCP-AFM) measurements. c) Current-voltage curves for (i) $(R\text{-}MBA)_2PbI_4$ and (ii) $(S\text{-}MBA)_2PbI_4$ thin films, where the tip is in non-magnetized, and with up and down magnetization directions. d) MR curves of devices based on (i) $(R\text{-}MBA)_2PbI_4$ and (ii) $(S\text{-}MBA)_2PbI_4$. Reproduced under terms of the CC-BY license.[19c] Copyright 2019, The Authors,

published by The American Association for the Advancement of Science. e) Spin-photogalvanic effect of (i) $(R\text{-}MBA)_2PbI_4$ and (ii) $(S\text{-}MBA)_2PbI_4$ shown in the curves of the in-plane photocurrent versus α, where α is the angle rotation of the quarter-wave plate along with its fast axis. Reproduced with permission.[75b] Copyright 2023, Royal Society of Chemistry.

Table 4. Several typical chiral-induced spin selectivity materials (CISSMs) and their spin polarizations measured using different methods.

CISSM	Spin polarization	Form	Measuring method
Double-stranded DNA[135]	60%	Monolayers	Photoelectron
Overcrowded alkenes[140]	43%	Films	mCP-AFM
Helicenes[136]	>40%	Monolayers	mCP-AFM
Superhelical polyaniline[138]	80%	Microfibers	mCP-AFM
3,5-dialkoxyphenyl derivatives of coronene bisimide and porphyrin[137]	>85%	Nanofibers	mCP-AFM
$(R/S\text{-}MBA)_2PbI_4$[19c]	>80%	Films	mCP-AFM
$(R/S\text{-}MBA)_2SnI_4$[5e]	94%	Films	mCP-AFM
$(R/S\text{-}MBA)_2CuX_4$, X = Cl, Br[19a]	90%	Films	mCP-AFM
Chiral molecular intercalation superlattices[139]	>60%	Films	Spin tunneling junctions
$(R/S\text{-}MePEA)_2PbI_4$[132]	—	Films	chiral-phonon-activated spin Seebeck effect
$(R/S\text{-}PEA)_2PbI_4$[10c]	—	Films	magneto-optical Kerr effect

5.2. Spin photovoltaics

The spin-photovoltaic function couples the spin transport and photovoltaic properties of spintronic materials to trigger innovative functionalities in spin photovoltaic devices (SPVs), such as the modulation of the output current and spin signals. As long as a spintronic material is used with photovoltaic properties and effective spin injection in the device, the spin-photovoltaic function can be realized, in theory. Based on C_{60} molecules, Sun et al. reported on the first spin-photovoltaic function and described the operation mechanism (**Figure 6**a-i).[15b] Due to typical vertical spin valve structure, both the spin valve effect and photovoltaic response could be realized independently. When a device is purely operated as a solar cell, the non-spin-polarized photogenerated carriers in the C_{60} layer will be driven by the built-in electric field between the two ferromagnetic electrodes. When the device is purely operated as a spin valve, the electrically injected current will flow in the direction opposite to the photogenerated current, and the output current can shift between high and low states by the magnetic field due to the

different coercivities of the two ferromagnetic electrodes. The detected open-circuit voltage will increase in the antiparallel case ($V_{oc,\ AP} > V_{oc,\ P}$), because a larger applied voltage will be required to offset the photogenerated current. When utilizing bias voltage and light intensity to separately modulate the injected spin-polarized current and photogenerated current, the magnetocurrent of this device can be tuned in a large range, from nearly zero to infinity, and such a device can also act as a perfect magnetic current inverter or a complex magnetic sensor, or even output a series of completely spin-polarized currents (Figure 6a-ii). Based on the above device principle, SPVs with similar functions have been subsequently realized in p-type organic small molecule H_2Pc[141] and OIHP $MAPbBr_3$.[56] Recently, to further improve spin photovoltaic performance, Qin et al. utilized an incomplete hetero-structure active layer composed of p- and n-type molecular semiconductors (P3HT and PTCDI-C13) to construct an SPV and trigger spin-photovoltaic performance. The spin-photovoltaic performance of this incomplete hetero-structure was enhanced by 15-fold compared to a single-component SPV.[142] Based on the structure of the active layer, the photovoltaic effect could be enhanced as much as possible under the requirement of maintaining effective spin transport. Nevertheless, the photovoltaic performance of the SPVs at this stage is still far from that of reported solar cells, and future efforts should focus on popular bulk heterojunction or interfacial modification. Regarding the spin photovoltaic function based on 2DMs, Xu et al. investigated the bulk spin photovoltaic effect in TMDCs, from a theoretical and computational stand point, revealing that TMDCs could be used to create spin current under light illumination.[143] Song et al. observed the spin photovoltaic effect in magnetic vdW heterostructures, which was composed of chromium triiodide (CrI_3) sandwiched between two graphene contacts. Specifically, the charge-transfer transitions between spin-polarized conduction and valence bands in CrI_3 were closely related to the helicity-dependent absorption of CrI_3, which finally led to the helicity-dependent spin photovoltaic effect (Figure 6b).[144] Accordingly, these results and mechanisms could be used to probe the magnetic order of CrI_3, which may be useful for investigating other 2D magnets.

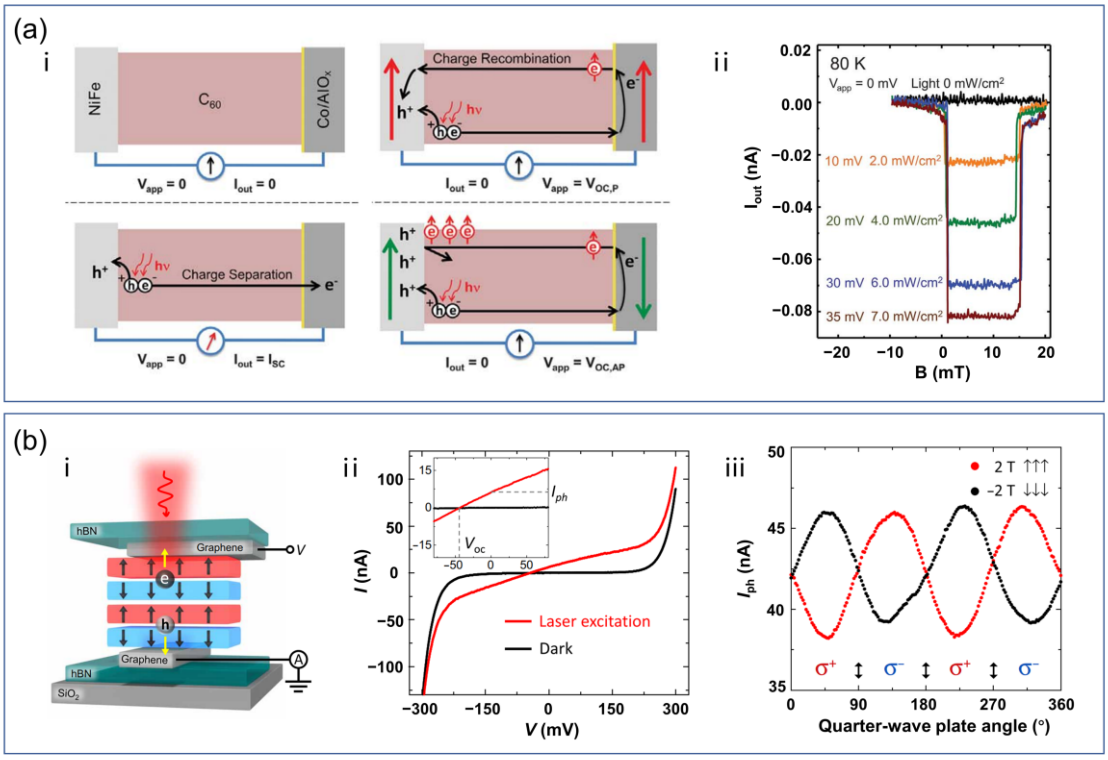

Figure 6. a) Spin-photovoltaic effect in a C_{60}-based spin-photovoltaic device: (i) operating principle, (ii) completely spin-polarized current output. Reproduced with permission.[15b] Copyright 2017, The American Association for the Advancement of Science. b) Spin-photovoltaic effect in magnetic van der Waals heterostructures of graphene contacts sandwiched with four-layer 2D magnet chromium triiodide (CrI_3); (i) schematic of the device structure; (ii) current-voltage curves of this device in the dark (black line) and under laser-excitation conditions (red line); (iii) photocurrent versus the quarter-wave plate angle at a fully spin-polarized state of 2 T and −2 T, exhibiting the circular polarization dependence of photocurrent. Reproduced under terms of the CC-BY license.[144] Copyright 2021, The Authors, published by The American Association for the Advancement of Science.

5.3. Spin Light Emitting Diodes

By integrating the spin transport and light-emitting properties of spintronic materials to construct spin-LED devices, we can achieve spin-LED functionality and modulate the electroluminescence (EL) efficiency by changing the relative spin polarization direction of the injected electrons and holes. Typically, carriers are electrically injected and polarized under ferromagnetic contacts or the sweeping magnetic field, with light or circularly polarized light finally emitted from the spin-polarized excitons. The EL intensity of the LED will strongly depend on the spin states of the injected carriers in this type of multipurpose spintronic device.

Traditional LED devices have a singlet/triplet ratio of 1:3, according to quantum statistics, with only singlets contributing to EL. Therefore, the maximum EL efficiency will be limited to 25%, in theory. By contrast, this ratio can be increased to 1:1 in a spin-LED device by modulating the injected electrons and holes in opposite spin states. Consequently, the theoretical maximum EL efficiency may be 50%. In fact, the largest obstacle to achieving spin-LED function is that the requisite EL turn-on voltage (V_{on}) (a few volts) will substantially exceed the threshold of the spin valve (less than 1 V). The first successful experiment was reported by Nguyen et al., where a spin-LED device was constructed based on a bipolar spin valve structure, and its intrinsic mechanism is shown in **Figure 7**a-i.[145] In this device, a thin LiF buffer layer was inserted at the interface to improve electron injection efficiency and a deuterated polymer D-DOO-PPV with a long spin lifetime was utilized as the spacer; therefore, V_{on} could be controlled to 3.5 V and a ~1% MEL was obtained at 10 K (Figure 7a-ii). In subsequent research, improving spin injection to decrease V_{on} or increase the threshold voltage of operating the spin valve was an important item of concern in spin-LED devices. By carefully inserting MoO_x and EIL at both FM/OSC interfaces to enhance electron and hole spin injection, Prieto-Ruiz et al. subsequently reported on an F8BT-based spin-LED with an enhanced MEL of 2.4% at 9 V, and at 20 K, the operating voltage of the spin valve surprisingly reached 14 V.[146] More recently, by first using the CISS mechanism of chiral OIHPs to realize spin-polarized hole injection, Kim et al. verified a spin-LED function based on 2D OIHPs ($CsPbX_3$ (where X was I or Br) nanocrystals), and the V_{on} was as low as 2.4 V.[19d] Due to >80% spin-polarized hole injection via the CISS of chiral metal-halide perovskite ($(R\text{-}MBA)_2PbI_4$ and $(S\text{-}MBA)_2PbI_4$), the researchers achieved highly external quantum efficiencies of more than 10% and an RT circularly polarized EL of ± 2.6% (Figure 7b). It should be noted that no external magnetic field was required in this entire operation process, providing an innovative strategy to achieve spin-LED functionality with both high-efficiency spin injection, low V_{on}, and the potential for device miniaturization. With respect to further improving the EL efficiency of spin-LED devices, the research direction should be semiconductor material design toward concurrent high EL efficiency and spin transport performance, and interface engineering toward high-efficiency spin injection. In addition, considering the current research states of spin-LED devices, many challenges still remain for their practical application in next-generation high-efficiency and low-consumption functional devices—in addition to EL efficiency—including operating temperature and the stability of working time and operating frequency.

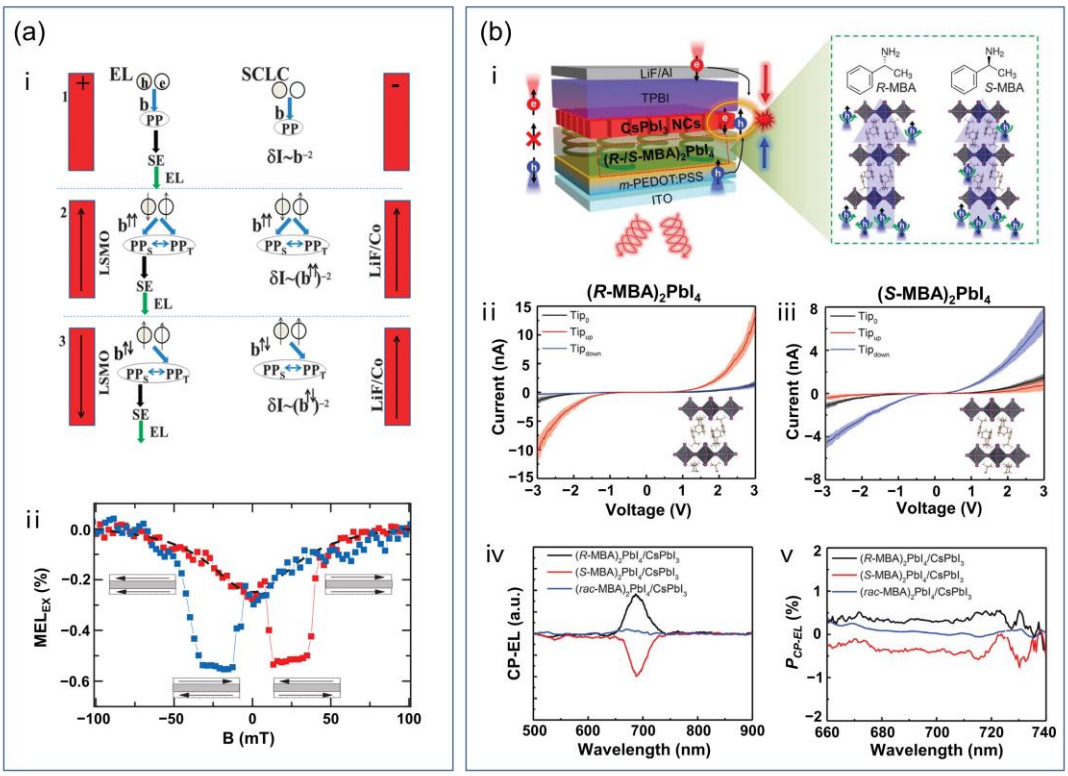

Figure 7. a) Spin light-emitting diodes (spin-LEDs) structured by LSMO/DOO-PPV/LiF/Co: (i) operating mechanism and (ii) magneto-electroluminescence performance. Reproduced with permission.[145] Copyright 2012, The American Association for the Advancement of Science. b) Spin-LED based on chiral-induced-spin-selectivity (CISS) materials: (i) schematic diagrams of the device structure and CISS materials, (ii, iii) current-voltage curves of the spin-LED with chiral (R-MBA)$_2$PbI$_4$ and (S-MBA)$_2$PbI$_4$ as the spin filter to produce spin-polarized current, measured by magnetic conductive-probe atomic force microscopy (mCP-AFM) at room temperature, (iv, v) characteristics of circularly polarized electroluminescence (CP-EL) and the EL polarization degree of this CISS material-based spin-LED. Reproduced with permission.[19d] Copyright 2021, The American Association for the Advancement of Science.

5.4. Spin-Transistor Function

The concept of a spin transistor was first proposed by Datta and Das in 1990, which was considered promising in data storage and information processing.[147] Benefiting from strong SOC in the two-dimensional electron gas (2DEG) of a narrow-gap semiconductor, the current flowing in the channel could be modulated by gate-voltage-controlled spin precession.[148] In spin transistors with this operating principle, the magnetic source and drain contacts were used for spin injection and detection, similar to the field-effect transistor, where the electrical gate could modulate the spin rotation during spin transport. Limited by material development, it was

not until 2009 that the first spin transistor in an InAs heterostructure was demonstrated by Koo et al., inspiring a wide range of research on realizing spin-transistor functionality based on 2DEG.[148a] To improve spin injection and investigate novel spin detection, several types of spin transistors based on this mechanism were reported.[148c, 149] However, almost all spin transistors based on this principle will only operate at low temperatures, due to the low spin injection efficiency and strong SOC of channel materials. In this review, 2DEG-based spin transistors will not be discussed extensively, as these material systems are beyond the scope of this review. Beyond coherent spin manipulation via 2DEG channel materials, the spin-transistor function can be extended to modulate spin current or MR signals in a broad sense. Directed at different channel materials, the principle to realizing spin-transistor function will be quite different.

In recent years, 2D vdW heterostructures with vertical stacking of different 2DM systems via vdW forces have provided a new operating principle for realizing spin-transistor function and are the key to next-generation computing technologies.[20b, 150] By integrating the long-distance spin transport properties of graphene and the strong SOC of MoS_2 in the 2D vdW heterostructure of graphene/MoS_2, Yan et al. first reported on the spin field-effect switch, whose operating temperature was 200 K, which was much higher than that of Datta-Das-like spin transistor.[105a] In this lateral spin valve, spin was injected into graphene from the FM source, diffused through the graphene/MoS_2 channel, and finally, non-locally detected by the FM drain. Since the gate voltage could control the amount of spin current absorbed by the MoS_2 layer before the spin current arrived at the drain terminal, a gate-tunable spin field-effect switch between binary ON and OFF could be achieved. Subsequently, Dankert et al. and other research groups demonstrated gate-tunable spin current and spin lifetime in graphene/MoS_2 vdW heterostructure systems at 300 K by measuring the gate-tunable spin valve signal and Hanle spin precession (**Figure 8**a).[116a] The researchers attributed this modulation to gate control on both the Schottky barriers at the graphene/MoS_2 interface and to MoS_2 conductivity, which promoted the understanding of gate-controllable spin relaxation in vdW heterostructure systems, offering an attractive route for future spin logic circuits and memory devices. Specifically, when the gate voltage (V_g) is swept toward negative values, the resistance of MoS_2 and the Schottky barriers at the graphene/MoS_2 interface were found to be extremely high, preventing the spin current in graphene from entering the MoS_2 channel. This condition allows the spins to smoothly transport in the graphene before they are detected, resulting in a spin-ON state. By contrast, when V_g is swept toward positive values, the resistance of MoS_2, as well as the Schottky barriers at the interface, will significantly decrease. In this case, the spin current in graphene will preferably enter MoS_2 and thus experience much faster spin relaxation due to

the strong SOC effect of MoS_2. Spin carriers will lose their orientation before reaching the drain, corresponding to a spin-OFF state. However, achieving a large high-low conductance ratio in these types of spin transistors still faces great challenges, due to the low spin injection efficiency and fast spin relaxation in the semiconductor channel. Despite the low ON/OFF ratio, these measurements shine a light on interfacial physical phenomena that may be otherwise difficult to investigate, such as the proximity effect, spin absorption, and subsequently (inverse) spin Hall effect and Rashba-Edelstein effect.[114e, 151] In addition to the above-mentioned spin-transistor function principle, recent discoveries of 2D magnetic materials, including chromium trihalides CrX_3 (where X = Cl, Br, or I),[152] $Cr_2Ge_2Te_6$, [153] Fe_3GeTe_2,[154] and vdW heterostructures based on these 2D magnetic materials have shown potential in exploiting spin-transistor function with novel principles. Jiang et al. constructed a spin tunnel field-effect transistor with a dual-gated graphene/CrI_3/graphene tunnel barrier structure, according to the electrical-field-controlled antiferromagnet-ferromagnet (FM-AFM) switching of bilayer CrI_3, and the device exhibited large gate-controlled and reversible conductance states, the high–low conductance ratio can approach 400%.[155] Through the assembly of the 2D ferromagnetic semiconductor Fe_3GeTe_2 with h-BN, Min et al. demonstrated electrically controllable TMR from −60% to 300% (Figure 8b). The researchers attributed the sign changes of TMR, i.e., reversal spin-polarized injection, to the electrically tunable spin-polarized electronic structure of Fe_3GeTe_2 from the low-energy itinerant to high-energy localized spin states.[154] These studies offer a promising route for obtaining electrically controllable spin-transistor functionality with a large modulation range.

For OSCs, the intrinsically weak SOC of OSCs suggested that it was difficult to realize spin-transistor function using the above-mentioned strategies. However, the unique spinterface effect between the ferromagnetic electrodes and the OSCs, and multipurpose device development, may provide a promising strategy to realize spin-transistor functions. In the present stage, this has only manifested in the final results of spin-transistor function, i.e., the modulation of spin current or MR. For the spinterface effect, interfacial hybridization between OSCs and the adjacent ferromagnetic electrode can form new hybrid interface states (HISs) through chemical adsorption.[156] Affected by such HISs, the spin-up and spin-down energy levels at the interface will be broadened, depending on the degree of interaction between the molecule and the electrode.[15c] However, the position of the energy levels can be spin-dependent shifted.[157] In both cases, a new DOS might appear at the E_F of the electrode, determining the spin polarization (p) of the injected current, which can be expressed as follows:

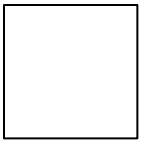

$$p = \frac{N_{\uparrow}(E_F) - N_{\downarrow}(E_F)}{N_{\uparrow}(E_F) + N_{\downarrow}(E_F)}, \quad (15)$$

where $N_{\uparrow}(E_F)$ and $N_{\downarrow}(E_F)$ are the amount of spin-up and spin-down electrons, respectively, at the Fermi level (E_F) of the electrode.[158] Considering that N is proportional to the DOS at the E_F of the electrode, HISs can provide effective spin polarization variation of the electrodes, leading to variations in the MR sign or the spin polarization of the injected spin current in the device, according to the Julliere formula.[15c, 156a, 157b, 159] According to the design concept of changing HISs, many investigations achieved MR with a change in sign or magnitude either by direct contact between the electrode and the OSCs or by inserting an interface layer. For example, Barraud et al. fabricated nanometer-scale LSMO/Alq_3/Co magnetic tunnel junctions (MTJs) by indenting the organic layer with an atomic force microscope tip. The obtained nanoscale MTJs exhibited impressive MR up to 300%. This positive MR sign was confusing when considering the commonly observed negative MR in relatively large-area devices with identical compositions. The abnormal MR effect was attributed to the formation of the HISs, which could lead to an increase in the effective spin polarization of the electrodes, or even a change in their sign.[15c] From the aspect of inserting an interfacial layer between the OSCs and FM electrodes to modify the interfacial properties and then the MR signals, to be specific, LiF as a common interface-modified material has been successfully used to tune the MR effect.[160] According to one explanation, the LiF dipolar layer can lead to a vacuum level shift and then change the energy level alignment between the OSCs and the FM electrodes, thereby reversing the spin polarization and the MR signals.[157a] According to another explanation, an antiferromagnetic layer will be generated at the interface due to a chemical reaction between LiF and the active FM metals, thus leading to a change in the MR sign.[161] In addition, interfacial layers with ferroelectricity, such as $PbZr_{0.2}Ti_{0.8}O_3$ (PZT)[162] and PVDF,[159] have also been employed to actively control the MR effect. Typically, Sun et al. fabricated OSVs with PZT as a ferroelectric interfacial layer and found that MR strongly depended on the electric polarization of the PZT layer, which could be actively controlled by an external electric field (Figure 8c-i).[162] Accordingly, the researchers proposed a model to explain these experimental results, as shown in Figure 8c-ii. The HOMO level of Alq_3 shifted via the dipole moment of the PZT layer, resulting in the shift of hole injection into the energy level deviating from the initial state of LSMO.

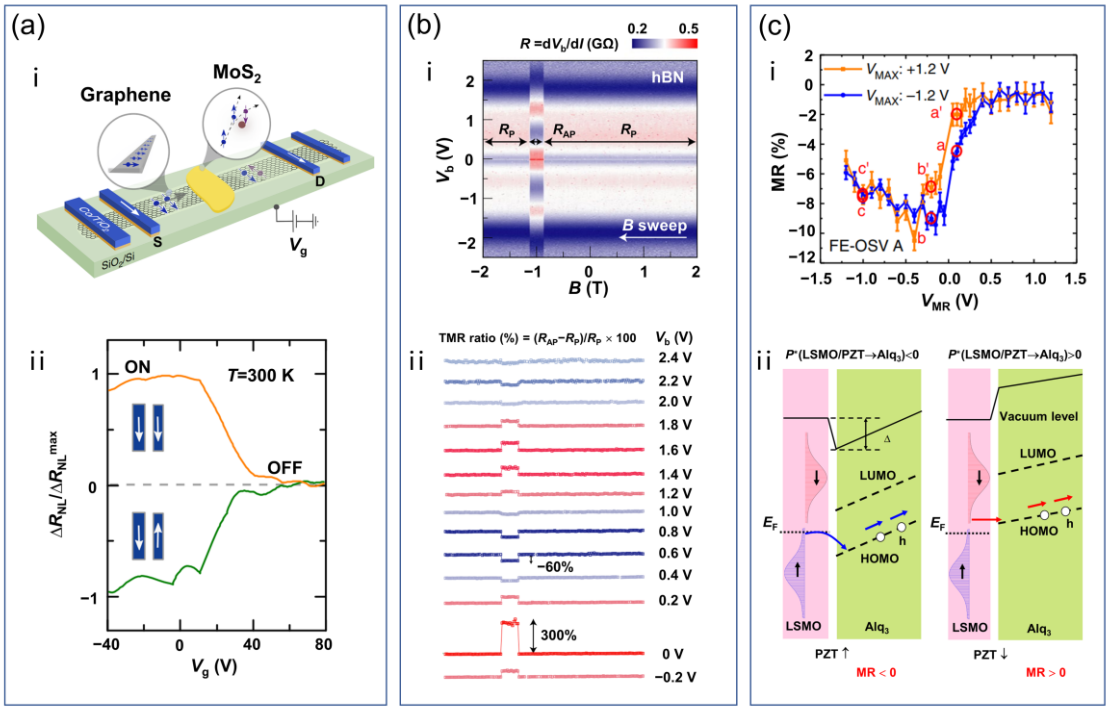

Figure 8. a) Spin-transistor function achieved in a graphene/MoS_2 vdW heterostructure: (i) schematic of graphene/MoS_2 vdW heterostructure spintronic device, (ii) measured gate-dependent ON/OFF spin signal modulation at room temperature. Reproduced with permission.[116a] Copyright 2017, The Authors, published by Springer Nature. b) Spin-transistor function in a vdW magnetic tunneling junction composed of ferromagnetic Fe_3GeTe_2 (FGT) with hexagonal boron nitride (hBN): (i) two-dimensional display of $R = dV_b/dI$ versus bias (V_b) under an out-of-plane magnetic field sweep, (ii) vertical stacks of tunneling magnetoresistance (TMR) curves at different biases from $V_b = 2.4$ V to −0.02 V, extracted from the datasets shown in Figure 8b-i. Reproduced with permission.[154] Copyright 2022, The Authors, published by Springer Nature. c) (i) Voltage-dependent magnetoresistance (MR) and (ii) model of MR change in the spin valve with the structure of LSMO/PZT/Alq_3/Co. Reproduced with permission.[162] Copyright 2014, The Authors, published by Springer Nature.

With the wide variety of OSCs and their unique response to external stimuli, it is of great significance for engineering organic/inorganic interfaces to obtain desired spin polarization and spin-transistor functions. However, due to the complexity of spinterfaces, research on the spinterface effect is still focusing on the scope of qualitative discussion, and quantitatively controlling the magnitude and sign of MR as a requirement of spinterface-based spin-transistor function remains a challenge. In the future, efforts should focus on innovation in materials, devices, mechanisms, experimental characterizations, and theoretical calculations. In terms of realizing spin-transistor function based on the multifunction of spintronic devices, spin-

photovoltaic device has been demonstrated, in which MR could be modulated from zero to infinity.[15b] A detailed description of this device can be found in Section 5.2. This example, based on novel device design, provides an avenue for developing innovative mechanisms of spin-transistor functions, and future related research may promote the development of spintronics.

6. Challenges and Prospective

In summary, the spin transport and spin manipulation in various promising materials and advanced spintronic devices are the core research contents on the roadmap of spintronics. In the review, we provided fundamental material introductions to OSCs, OIHPs, and 2DMs, and their spin-related merits and opportunities were carefully analyzed and discussed. Significant achievements have been made in the understanding and optimization of the spin transport properties of materials and devices. Several approaches have been testified, at least at the fundamental research level, to realize spin manipulation. These include the traditional path of enhancing SOC coupling through virous techniques and the more novel strategy of implementing spin manipulation with chirality or valley selectivity. We indeed confront challenges, and along with that, the exciting opportunities for the research field. From the perspective of material selection, a long spin lifetime and relaxation length are desirable for both spin transport and spin manipulation, with a strong SOC or Rashba effect particularly important for spin manipulation. Nevertheless, even with an understanding of the materials requirement for optimum spintronic devices, the current research does not provide sufficient scientific basis guide the selection or design of spintronic materials. For example, the knowledge on chemical structure, aggregation or crystal structure, and doping of materials will certainly influence the ability to select and design spintronic materials. It is still ambiguous and partial in both theory and experiment regarding how to control these factors for optimum spintronic performances. Most spintronic devices based on 2D materials, either new proof-of-concept devices or devices with more established architecture, are based on mechanically exfoliated flakes. Although reported spintronic material parameters from different research groups do tend to fall within a certain range statistically, exact reproducibility is limited by the nature of the fabrication process and will remain poor until significant progress is made in materials science. Research in epitaxial growth of 2D materials, which is already accelerating at a significant pace, will help overcoming the material bottleneck and permitting quantitative study of 2D spintronic devices. To facilitate the development in this area, more efforts in both theories and experiments is required at the most fundamental level, such as the investigations

of the relationship between chemical, physical structure and spin lifetime, spin diffusion length, SOC or Rashba strength.

The use and development of various detection techniques and the collaboration among expertise in different subject areas will greatly help the understanding of fundamental issues. For example, direct probing of spin transport and relaxation using different techniques beside transport measurement, such as low-energy muon spin rotation,[163] two-photon photoemission measurement.[164] It is particularly helpful if the technique can provide temporal resolution to provide insight to the dynamics of spin relaxation, and therefore can help to identify the causes of spin relaxation. Such techniques include for example, electron paramagnetic resonance technique,[165] ultrafast optics[166] etc. The device fabrication process should be improved to enhance the reproducibility of device performance. Indeed, successful designs and fabrications of spintronic devices remains the challenge because they require a whole range of considerations on material and interfacial properties, and chemical competitively etc. In particular, the electrical probing of spin-polarized properties is far more challenging than its optical counterpart because spins in electrical devices will require optimized environment during the whole complete process of injection, transport, manipulation and detection. As a result of the requirement for high-quality interface for spin injection and detection in a device, it is eagerly important to develop advanced preparation methods for both intermediate materials and top/bottom ferromagnetic electrodes. With regard to spin manipulation, effective uses of SOC, Rashba effect, and CISS for diversified hybrid perovskites are of critical importance. Innovative approaches for spin manipulation are as important as materials optimization, in particularly, there is rarely report of spin manipulation in OIHPs, especially electrically controlled, although OIHPs possess strong SOC.

For the further functional application of these spintronic materials, hybrid devices exploiting superior spintronic properties of various systems among OSCs, OIHPs, and 2DMs will be attractive. A combination of electrical and optical manipulation of spin transport in the ultrafast time regime will be even more appealing for the development of new, multi-functional, fast and energy efficient opto-spintronic devices. Finally, relevant theories regarding spin transport and manipulation should always keep pace with experiments, to provide rational predictions and thorough explanations.

Acknowledgements

L.G. and S.H. contributed equally to this work. This work is supported financially by the National Natural Science Foundation of China (Grant Nos. 52250008, 52050171, 51973043,

22175047, 52103203, 52103338 and 91963126), the Strategic Priority Research Program of the Chinese Academy of Sciences (Grant No. XDB36020000), the Ministry of Science and Technology of the People's Republic of China (2017YFA0206600), the CAS Instrument Development Project (Grant No. YJKYYQ20170037), the Beijing Natural Science Foundation (Grant Nos. 4222087, 2222086) and Shandong Province (Grant No. ZR2020ME070), the China Postdoctoral Science Foundation (Grant Nos. 2021M690802,), the Beijing National Laboratory for Molecular Sciences (Grant No. BNLMS201907), and the CAS Pioneer Hundred Talents Program. W. Y. is supported by Anne McLaren Fellowship from the University of Nottingham, Royal Society Research Grant RGS\R2\212207 and the University of Nottingham Propulsion Futures Beacon.

Conflict of Interest

All the authors declare that they have no conflict of interest.

Received: ((will be filled in by the editorial staff))
Revised: ((will be filled in by the editorial staff))
Published online: ((will be filled in by the editorial staff))

References

[1] a) M. N. Baibich, J. M. Broto, A. Fert, F. Nguyen Van Dau, F. Petroff, P. Etienne, G. Creuzet, A. Friederich, J. Chazelas, *Phys. Rev. Lett.* **1988**, *61*, 2472; b) G. Binasch, P. Grunberg, F. Saurenbach, W. Zinn, *Phys. Rev. B* **1989**, *39*, 4828; c) A. Fert, *Rev. Mod. Phys.* **2008**, *80*, 1517.

[2] a) S. A. Wolf, D. D. Awschalom, R. A. Buhrman, J. M. Daughton, S. von Molnar, M. L. Roukes, A. Y. Chtchelkanova, D. M. Treger, *Science* **2001**, *294*, 1488; b) S. Parkin, S.-H. Yang, *Nat. Nanotechnol.* **2015**, *10*, 195; c) C. Chappert, A. Fert, F. N. Van Dau, *Nat. Mater.* **2007**, *6*, 813; d) G. A. Prinz, *Science* **1998**, *282*, 1660; e) P. A. Bobbert, *Science* **2014**, *345*, 1450.

[3] a) X. Zhang, H. Dong, W. Hu, *Adv. Mater.* **2018**, *30*, 1801048; b) C. Wang, H. Dong, L. Jiang, W. Hu, *Chem. Soc. Rev.* **2018**, *47*, 422; c) A. R. Mellnik, J. S. Lee, A. Richardella, J. L. Grab, P. J. Mintun, M. H. Fischer, A. Vaezi, A. Manchon, E. A. Kim, N. Samarth, D. C. Ralph, *Nature* **2014**, *511*, 449; d) Y. Jung, M. S. Choi, A. Nipane, A. Borah, B. Kim, A. Zangiabadi, T. Taniguchi, K. Watanabe, W. J. Yoo, J. Hone, J. T. Teherani, *Nat. Electron.* **2019**, *2*, 187; e) J. Shin, H. Kim, S. Sundaram, J. Jeong, B. I. Park, C. S. Chang, J. Choi, T. Kim, M. Saravanapavanantham, K. Lu, S. Kim, J. M. Suh, K. S. Kim, M. K. Song, Y. Liu, K. Qiao, J.

H. Kim, Y. Kim, J. H. Kang, J. Kim, D. Lee, J. Lee, J. S. Kim, H. E. Lee, H. Yeon, H. S. Kum, S. H. Bae, V. Bulovic, K. J. Yu, K. Lee, K. Chung, Y. J. Hong, A. Ougazzaden, J. Kim, *Nature* **2023**, *614*, 81; f) A. W. Tsen, B. Hunt, Y. D. Kim, Z. J. Yuan, S. Jia, R. J. Cava, J. Hone, P. Kim, C. R. Dean, A. N. Pasupathy, *Nat. Phys.* **2015**, *12*, 208; g) G. Liu, Z. Tian, Z. Yang, Z. Xue, M. Zhang, X. Hu, Y. Wang, Y. Yang, P. K. Chu, Y. Mei, L. Liao, W. Hu, Z. Di, *Nat. Electron.* **2022**, *5*, 275; h) D. Hsieh, D. Qian, L. Wray, Y. Xia, Y. S. Hor, R. J. Cava, M. Z. Hasan, *Nature* **2008**, *452*, 970; i) T. D. Ladd, F. Jelezko, R. Laflamme, Y. Nakamura, C. Monroe, J. L. O'Brien, *Nature* **2010**, *464*, 45; j) L. Veyrat, C. Deprez, A. Coissard, X. X. Li, F. Gay, K. Watanabe, T. Taniguchi, Z. Han, B. A. Piot, H. Sellier, B. Sacepe, *Science* **2020**, *367*, 781; k) M. J. Stevens, A. L. Smirl, R. D. Bhat, A. Najmaie, J. E. Sipe, H. M. Van Driel, *Phys. Rev. Lett.* **2003**, *90*, 136603; l) A. Saraiva-Souza, M. Smeu, L. Zhang, A. G. Souza Filho, H. Guo, M. A. Ratner, *J. Am. Chem. Soc.* **2014**, *136*, 15065; m) Z. Jiang, C. Z. Chang, M. R. Masir, C. Tang, Y. Xu, J. S. Moodera, A. H. MacDonald, J. Shi, *Nat. Commun.* **2016**, *7*, 11458; n) D. Khokhriakov, A. M. Hoque, B. Karpiak, S. P. Dash, *Nat. Commun.* **2020**, *11*, 3657; o) C. Felser, G. H. Fecher, B. Balke, *Angew. Chem. Int. Ed.* **2007**, *46*, 668; p) D. Li, G. Yu, *Adv. Funct. Mater.* **2021**, *31*, 2100550; q) X. L. Wang, S. X. Dou, C. Zhang, *NPG Asia Mater.* **2010**, *2*, 31; r) P. Bujak, I. Kulszewicz-Bajer, M. Zagorska, V. Maurel, I. Wielgus, A. Pron, *Chem. Soc. Rev.* **2013**, *42*, 8895; s) K. Liao, X. Hu, Y. Cheng, Z. Yu, Y. Xue, Y. Chen, Q. Gong, *Adv. Optical Mater.* **2019**, *7*, 1900350.

[4] a) B. Dieny, I. L. Prejbeanu, K. Garello, P. Gambardella, P. Freitas, R. Lehndorff, W. Raberg, U. Ebels, S. O. Demokritov, J. Akerman, A. Deac, P. Pirro, C. Adelmann, A. Anane, A. V. Chumak, A. Hirohata, S. Mangin, S. O. Valenzuela, M. C. Onbaşlı, M. d'Aquino, G. Prenat, G. Finocchio, L. Lopez-Diaz, R. Chantrell, O. Chubykalo-Fesenko, P. Bortolotti, *Nat. Electron.* **2020**, *3*, 446; b) I. Zutic, J. Fabian, S. Das Sarma, *Rev. Mod. Phys.* **2004**, *76*, 323.

[5] a) X. Li, j. Yang, *Natl. Sci. Rev.* **2016**, *3*, 365; b) B. Dlubak, M.-B. Martin, C. Deranlot, B. Servet, S. Xavier, R. Mattana, M. Sprinkle, C. Berger, W. A. De Heer, F. Petroff, A. Anane, P. Seneor, A. Fert, *Nat. Phys.* **2012**, *8*, 557; c) X. Du, I. Skachko, A. Barker, E. Y. Andrei, *Nat. Nanotechnol.* **2008**, *3*, 491; d) M. Gurram, S. Omar, B. J. van Wees, *2D Mater.* **2018**, *5*, 032004; e) H. Lu, C. Xiao, R. Song, T. Li, A. E. Maughan, A. Levin, R. Brunecky, J. J. Berry, D. B. Mitzi, V. Blum, M. C. Beard, *J. Am. Chem. Soc.* **2020**, *142*, 13030; f) M. I. Miah, E. M. Gray, *Solid State Sciences* **2008**, *10*, 205; g) K. Wang, Q. Yang, J. Duan, C. Zhang, F. Zhao, H. Yu, B. Hu, *Adv. Mater. Interfaces* **2019**, *6*, 1900718; h) X. Zhang, S. Mizukami, T. Kubota, Q. Ma, M. Oogane, H. Naganuma, Y. Ando, T. Miyazaki, *Nat. Commun.* **2013**, *4*, 1392; i) L. Guo, Y. Qin, X. Gu, X. Zhu, Q. Zhou, X. Sun, *Front. Chem.* **2019**, *7*, 428; j) O. M. van 't Erve, A. L.

Friedman, C. H. Li, J. T. Robinson, J. Connell, L. J. Lauhon, B. T. Jonker, *Nat. Commun.* **2015**, *6*, 7541; k) Y. Zhu, L. Guo, J. Guo, L. Zhao, C. Li, X. Qiu, Y. Qin, X. Gu, X. Sun, Z. Tang, *Angew. Chem. Int. Ed.* **2023**, *62*, e202213208.

[6] a) I. Appelbaum, B. Huang, D. J. Monsma, *Nature* **2007**, *447*, 295; b) D. Chiba, M. Sawicki, Y. Nishitani, Y. Nakatani, F. Matsukura, H. Ohno, *Nature* **2008**, *455*, 515; c) X.-R. Gu, L.-D. Guo, X.-N. Sun, *Chin. Phys. B* **2018**, *27*, 107202; d) A. M. Tyryshkin, S. A. Lyon, W. Jantsch, F. Schäffler, *Phys. Rev. Lett.* **2005**, *94*, 126802; e) N. Lambert, I. Mahboob, M. Pioro-Ladriere, Y. Tokura, S. Tarucha, H. Yamaguchi, *Phys. Rev. Lett.* **2008**, *100*, 136802; f) B. Nafradi, M. Choucair, K. P. Dinse, L. Forro, *Nat. Commun.* **2016**, *7*, 12232; g) R. Hanson, D. D. Awschalom, *Nature* **2008**, *453*, 1043; h) A. M. Tyryshkin, S. A. Lyon, W. Jantsch, F. Schaffler, *Phys. Rev. Lett.* **2005**, *94*, 126802.

[7] a) F. Casper, T. Graf, S. Chadov, B. Balke, C. Felser, *Semicond. Sci. Technol.* **2012**, *27*, 063001; b) T. Jungwirth, J. Sinova, J. Mašek, J. Kučera, A. H. MacDonald, *Rev. Mod. Phys.* **2006**, *78*, 809; c) S. J. Pearton, W. H. Heo, M. Ivill, D. P. Norton, T. Steiner, *Semicond. Sci. Technol.* **2004**, *19*, R59.

[8] a) Z. H. Xiong, D. Wu, Z. V. Vardeny, J. Shi, *Nature* **2004**, *427*, 821; b) S. Sanvito, *Nat. Mater.* **2007**, *6*, 803; c) A. Cornia, P. Seneor, *Nat. Mater.* **2017**, *16*, 505; d) Y. Zhang, L. Guo, X. Zhu, X. Sun, *Front. Chem.* **2020**, *8*, 589207; e) J. Devkota, R. Geng, R. C. Subedi, T. D. Nguyen, *Adv. Funct. Mater.* **2016**, *26*, 3881; f) V. A. Dediu, L. E. Hueso, I. Bergenti, C. Taliani, *Nat. Mater.* **2009**, *8*, 707; g) H. J. Jang, C. A. Richter, *Adv. Mater.* **2017**, *29*, 1602739; h) D. Sun, E. Ehrenfreund, Z. V. Vardeny, *Chem. Commun.* **2014**, *50*, 1781; i) T. Sugawara, M. M. Matsushita, *J. Mater. Chem.* **2009**, *19*, 1738.

[9] a) Z. V. Vardeny, H. Guo, C. Zhang, X. Pan, J. Wang, *J. Photonics Energy* **2018**, *8*, 032207; b) J. Wang, C. Zhang, H. Liu, X. Liu, H. Guo, D. Sun, Z. V. Vardeny, *Adv. Mater.* **2019**, *31*, e1904059; c) Y. Lu, Q. Wang, R. Chen, L. Qiao, F. Zhou, X. Yang, D. Wang, H. Cao, W. He, F. Pan, Z. Yang, C. Song, *Adv. Funct. Mater.* **2021**, *31*, 2104605; d) A. Privitera, M. Righetto, F. Cacialli, M. K. Riede, *Adv. Optical Mater.* **2021**, *9*, 2100215.

[10] a) W. Han, R. K. Kawakami, M. Gmitra, J. Fabian, *Nat. Nanotechnol.* **2014**, *9*, 794; b) Y. Liu, Y. Huang, X. Duan, *Nature* **2019**, *567*, 323; c) Z. Huang, B. P. Bloom, X. Ni, Z. N. Georgieva, M. Marciesky, E. Vetter, F. Liu, D. H. Waldeck, D. Sun, *ACS Nano* **2020**, *14*, 10370; d) C. Liu, H. Chen, S. Wang, Q. Liu, Y. G. Jiang, D. W. Zhang, M. Liu, P. Zhou, *Nat. Nanotechnol.* **2020**, *15*, 545; e) X. Lin, W. Yang, K. L. Wang, W. Zhao, *Nat. Electron.* **2019**, *2*, 274.

[11] a) M. W. Wu, J. H. Jiang, M. Q. Weng, *Phys. Rep.* **2010**, *493*, 61; b) B. Huang, H.-J. Jang, I. Appelbaum, *Appl. Phys. Lett.* **2008**, *93*, 162508; c) M. B. Lundeberg, R. Yang, J. Renard, J. A. Folk, *Phys. Rev. Lett.* **2013**, *110*, 156601; d) A. Kiss, L. Szolnoki, F. Simon, *Sci. Rep.* **2016**, *6*, 22706; e) L. Nuccio, M. Willis, L. Schulz, S. Fratini, F. Messina, M. D'Amico, F. L. Pratt, J. S. Lord, I. McKenzie, M. Loth, B. Purushothaman, J. Anthony, M. Heeney, R. M. Wilson, I. Hernandez, M. Cannas, K. Sedlak, T. Kreouzis, W. P. Gillin, C. Bernhard, A. J. Drew, *Phys. Rev. Lett.* **2013**, *110*, 216602; f) R. C. Roundy, M. E. Raikh, *Phys. Rev. B* **2014**, *90*, 201203(R); g) Z. G. Yu, *Phys. Rev. Lett.* **2011**, *106*, 106602.

[12] C. A. Masmanidis, H. H. Jaffe, R. L. Ellis, *J. Phys. Chem.* **1975**, *79*, 2052.

[13] S. Y. Lee, S. Y. Paik, D. R. McCamey, J. Yu, P. L. Burn, J. M. Lupton, C. Boehme, *J. Am. Chem. Soc.* **2011**, *133*, 2019.

[14] a) A. Manchon, H. C. Koo, J. Nitta, S. M. Frolov, R. A. Duine, *Nat. Mater.* **2015**, *14*, 871; b) H. C. Koo, S. B. Kim, H. Kim, T. E. Park, J. W. Choi, K. W. Kim, G. Go, J. H. Oh, D. K. Lee, E. S. Park, I. S. Hong, K. J. Lee, *Adv. Mater.* **2020**, *32*, 2002117.

[15] a) X. Sun, A. Bedoya-Pinto, Z. Mao, M. Gobbi, W. Yan, Y. Guo, A. Atxabal, R. Llopis, G. Yu, Y. Liu, A. Chuvilin, F. Casanova, L. E. Hueso, *Adv. Mater.* **2016**, *28*, 2609; b) X. Sun, S. Vélez, A. Atxabal, A. Bedoya-Pinto, S. Parui, X. Zhu, R. Llopis, F. Casanova, L. E. Hueso, *Science* **2017**, *357*, 677; c) C. Barraud, P. Seneor, R. Mattana, S. Fusil, K. Bouzehouane, C. Deranlot, P. Graziosi, L. Hueso, I. Bergenti, V. Dediu, F. Petroff, A. Fert, *Nat. Phys.* **2010**, *6*, 615.

[16] a) S. Colella, E. Mosconi, P. Fedeli, A. Listorti, F. Gazza, F. Orlandi, P. Ferro, T. Besagni, A. Rizzo, G. Calestani, G. Gigli, F. De Angelis, R. Mosca, *Chem. Mater.* **2013**, *25*, 4613; b) M. Zhou, J. S. Sarmiento, C. Fei, X. Zhang, H. Wang, *J. Phys. Chem. Lett.* **2020**, *11*, 1502.

[17] a) Y. X. Zhai, S. Baniya, C. Zhang, J. W. Li, P. Haney, C. X. Sheng, E. Ehrenfreund, Z. V. Vardeny, *Sci. Adv.* **2017**, *3*, e1700704; b) S. D. Stranks, P. Plochocka2, *Nat. Mater.* **2018**, *18*, 377; c) D. Niesner, M. Wilhelm, I. Levchuk, A. Osvet, S. Shrestha, M. Batentschuk, C. Brabec, T. Fauster, *Phys. Rev. Lett.* **2016**, *117*, 126401; d) E. Lafalce, E. Amerling, Z. G. Yu, P. C. Sercel, L. Whittaker-Brooks, Z. V. Vardeny, *Nat. Commun.* **2022**, *13*, 483.

[18] a) S.-H. Yang, R. Naaman, Y. Paltiel, S. S. P. Parkin, *Nat. Rev. Phys.* **2021**, *3*, 328; b) V. Kiran, S. P. Mathew, S. R. Cohen, I. H. Delgado, J. Lacour, R. Naaman, *Adv. Mater.* **2016**, *28*, 1957; c) Y. Kunihashi, H. Sanada, H. Gotoh, K. Onomitsu, M. Kohda, J. Nitta, T. Sogawa, *Nat. Commun.* **2016**, *7*, 10722; d) Z. G. Yu, *J. Phys. Chem. Lett.* **2020**, *11*, 8638; e) R. Naaman, Y. Paltiel, D. H. Waldeck, *J. Phys. Chem. Lett.* **2020**, *11*, 3660; f) R. Naaman, Y. Paltiel, D. H. Waldeck, *Nat. Rev. Chem.* **2019**, *3*, 250.

[19] a) Y. Lu, Q. Wang, R. He, F. Zhou, X. Yang, D. Wang, H. Cao, W. He, F. Pan, Z. Yang, C. Song, *Angew. Chem. Int. Ed.* **2021**, *60*, 23578; b) J. Ma, H. Wang, D. Li, *Adv. Mater.* **2021**, *33*, e2008785; c) H. P. Lu, J. Y. Wang, C. X. Xiao, X. Pan, X. H. Chen, R. Brunecky, J. J. Berry, K. Zhu, M. C. Beard, Z. V. Vardeny, *Sci. Adv.* **2019**, *5*, 2104605; d) Y. H. Kim, Y. X. Zhai, H. P. Lu, X. Pan, C. X. Xiao, E. A. Gaulding, S. P. Harvey, J. J. Berry, Z. V. Vardeny, J. M. Luther, M. C. Beard, *Science* **2021**, *371*, 1129; e) Y. Dong, Y. Zhang, X. Li, Y. Feng, H. Zhang, J. Xu, *Small* **2019**, *15*, e1902237.

[20] a) M. Gmitra, J. Fabian, *Phys. Rev. B* **2015**, *92*, 155403; b) J. F. Sierra, J. Fabian, R. K. Kawakami, S. Roche, S. O. Valenzuela, *Nat. Nanotechnol.* **2021**, *16*, 856; c) B. Huang, M. A. McGuire, A. F. May, D. Xiao, P. Jarillo-Herrero, X. Xu, *Nat. Mater.* **2020**, *19*, 1276.

[21] F. Evers, A. Aharony, N. Bar-Gill, O. Entin-Wohlman, P. Hedegard, O. Hod, P. Jelinek, G. Kamieniarz, M. Lemeshko, K. Michaeli, V. Mujica, R. Naaman, Y. Paltiel, S. Refaely-Abramson, O. Tal, J. Thijssen, M. Thoss, J. M. van Ruitenbeek, L. Venkataraman, D. H. Waldeck, B. Yan, L. Kronik, *Adv. Mater.* **2022**, *34*, e2106629.

[22] a) F. Zhang, H. Lu, J. Tong, J. J. Berry, M. C. Beard, K. Zhu, *Energy Environ. Sci.* **2020**, *13*, 1154; b) A. K. Jena, A. Kulkarni, T. Miyasaka, *Chem. Rev.* **2019**, *119*, 3036; c) F. Xia, H. Wang, D. Xiao, M. Dubey, A. Ramasubramaniam, *Nat. Photon.* **2014**, *8*, 899; d) R. Lv, J. A. Robinson, R. E. Schaak, D. Sun, Y. Sun, T. E. Mallouk, M. Terrones, *Acc. Chem. Res.* **2015**, *48*, 56; e) F. H. Koppens, T. Mueller, P. Avouris, A. C. Ferrari, M. S. Vitiello, M. Polini, *Nat. Nanotechnol.* **2014**, *9*, 780.

[23] C. Boehme, J. M. Lupton, *Nat. Nanotechnol.* **2013**, *8*, 612.

[24] a) S. Pramanik, C. G. Stefanita, S. Patibandla, S. Bandyopadhyay, K. Garre, N. Harth, M. Cahay, *Nat. Nanotechnol.* **2007**, *2*, 216; b) S. Watanabe, K. Ando, K. Kang, S. Mooser, Y. Vaynzof, H. Kurebayashi, E. Saitoh, H. Sirringhaus, *Nat. Phys.* **2014**, *10*, 308.

[25] S. Sanvito, *Chem. Soc. Rev.* **2011**, *40*, 3336.

[26] a) Y. J. Cheng, S. H. Yang, C. S. Hsu, *Chem. Rev.* **2009**, *109*, 5868; b) S. Gunes, H. Neugebauer, N. S. Sariciftci, *Chem. Rev.* **2007**, *107*, 1324; c) G. Li, R. Zhu, Y. Yang, *Nat. Photon.* **2012**, *6*, 153; d) B. C. Thompson, J. M. Frechet, *Angew. Chem. Int. Ed.* **2008**, *47*, 58; e) R. H. Friend, R. W. Gymer, A. B. Holmes, J. H. Burroughes, R. N. Marks, C. Taliani, D. D. C. Bradley, D. A. Dos Santos, J. L. Bredas, M. Logdlund, W. R. Salaneck, *Nature* **1999**, *397*, 121; f) M. S. Alsalhi, J. Alam, L. A. Dass, M. Raja, *Int. J. Mol. Sci.* **2011**, *12*, 2036; g) Y. Shirota, H. Kageyama, *Chem. Rev.* **2007**, *107*, 953; h) C. Wang, H. Dong, W. Hu, Y. Liu, D. Zhu, *Chem. Rev.* **2012**, *112*, 2208; i) A. Facchetti, *Chem. Mater.* **2010**, *23*, 733.

[27] a) L. Guo, X. Zhu, S. Sun, C. Cong, Q. Zhou, X. Sun, Y. Liu, *Org. Electron.* **2019**, *69*, 308; b) X. Sun, A. Bedoya-Pinto, R. Llopis, F. Casanova, L. E. Hueso, *Appl. Phys. Lett.* **2014**, *105*, 083302; c) Y. Zhao, A. Gumyusenge, J. He, G. Qu, W. W. McNutt, Y. Long, H. Zhang, L. Huang, Y. Diao, J. Mei, *Adv. Funct. Mater.* **2018**, *28*, 1705584; d) J. Y. Oh, S. Rondeau-Gagne, Y. C. Chiu, A. Chortos, F. Lissel, G. N. Wang, B. C. Schroeder, T. Kurosawa, J. Lopez, T. Katsumata, J. Xu, C. Zhu, X. Gu, W. G. Bae, Y. Kim, L. Jin, J. W. Chung, J. B. Tok, Z. Bao, *Nature* **2016**, *539*, 411.

[28] a) P. A. Bobbert, T. D. Nguyen, W. Wagemans, F. W. A. van Oost, B. Koopmans, M. Wohlgenannt, *Synth. Met.* **2010**, *160*, 223; b) Z. G. Yu, *Phys. Rev. B* **2012**, *85*, 115201; c) J. Rybicki, M. Wohlgenannt, *Phys. Rev. B* **2009**, *79*, 153202; d) T. D. Nguyen, Y. Sheng, J. Rybicki, G. Veeraraghavan, M. Wohlgenannt, *J. Mater. Chem.* **2007**, *17*, 1995; e) P. A. Bobbert, *Nat. Mater.* **2010**, *9*, 288; f) D. R. McCamey, K. J. van Schooten, W. J. Baker, S. Y. Lee, S. Y. Paik, J. M. Lupton, C. Boehme, *Phys. Rev. Lett.* **2010**, *104*, 017601; g) T. D. Nguyen, G. Hukic-Markosian, F. Wang, L. Wojcik, X. G. Li, E. Ehrenfreund, Z. V. Vardeny, *Nat. Mater.* **2010**, *9*, 345; h) T. D. Nguyen, G. Hukic-Markosian, F. Wang, L. Wojcik, X.-G. Li, E. Ehrenfreund, Z. V. Vardeny, *Synth. Met.* **2011**, *161*, 598; i) Y. Sheng, T. D. Nguyen, G. Veeraraghavan, Ö. Mermer, M. Wohlgenannt, S. Qiu, U. Scherf, *Phys. Rev. B* **2006**, *74*, 045213; j) Z. G. Yu, F. Ding, H. Wang, *Phys. Rev. B* **2013**, *87*, 205446.

[29] a) S. Schott, E. R. McNellis, C. B. Nielsen, H. Y. Chen, S. Watanabe, H. Tanaka, I. McCulloch, K. Takimiya, J. Sinova, H. Sirringhaus, *Nat. Commun.* **2017**, *8*, 15200; b) D. Sun, K. J. van Schooten, M. Kavand, H. Malissa, C. Zhang, M. Groesbeck, C. Boehme, Z. Valy Vardeny, *Nat. Mater.* **2016**, *15*, 863.

[30] S. Liang, R. Geng, B. Yang, W. Zhao, R. Chandra Subedi, X. Li, X. Han, T. D. Nguyen, *Sci. Rep.* **2016**, *6*, 19461.

[31] M. Gobbi, F. Golmar, R. Llopis, F. Casanova, L. E. Hueso, *Adv. Mater.* **2011**, *23*, 1609.

[32] F. Li, T. Li, F. Chen, F. Zhang, *Sci. Rep.* **2015**, *5*, 9355.

[33] M. Ding, X. Gu, L. Guo, R. Zhang, X. Zhu, R. Li, X. Zhang, W. Hu, X. Sun, *J. Mater. Chem. C* **2022**, *10*, 2507.

[34] J. Tsurumi, H. Matsui, T. Kubo, R. Häusermann, C. Mitsui, T. Okamoto, S. Watanabe, J. Takeya, *Nat. Phys.* **2017**, *13*, 994.

[35] a) S. Wang, D. Venkateshvaran, M. R. Mahani, U. Chopra, E. R. McNellis, R. Di Pietro, S. Schott, A. Wittmann, G. Schweicher, M. Cubukcu, K. Kang, R. Carey, T. J. Wagner, J. N. M. Siebrecht, D. P. G. H. Wong, I. E. Jacobs, R. O. Aboljadayel, A. Ionescu, S. A. Egorov, S. Mueller, O. Zadvorna, P. Skalski, C. Jellett, M. Little, A. Marks, I. McCulloch, J. Wunderlich,

J. Sinova, H. Sirringhaus, *Nat. Electron.* **2019**, *2*, 98; b) Z. G. Yu, *Phys. Rev. Lett.* **2013**, *111*, 016601.

[36] X. Sun, M. Gobbi, A. Bedoya-Pinto, O. Txoperena, F. Golmar, R. Llopis, A. Chuvilin, F. Casanova, L. E. Hueso, *Nat. Commun.* **2013**, *4*, 2794.

[37] S. Ding, Y. Tian, H. Wang, Z. Zhou, W. Mi, Z. Ni, Y. Zou, H. Dong, H. Gao, D. Zhu, W. Hu, *ACS Nano* **2018**, *12*, 12657.

[38] Z. G. Yu, *Nat. Commun.* **2014**, *5*, 4842.

[39] S. W. Jiang, S. Liu, P. Wang, Z. Z. Luan, X. D. Tao, H. F. Ding, D. Wu, *Phys. Rev. Lett.* **2015**, *115*, 086601.

[40] W. Yang, Q. Shi, T. Miao, Q. Li, P. Cai, H. Liu, H. Lin, Y. Bai, Y. Zhu, Y. Yu, L. Deng, W. Wang, L. Yin, D. Sun, X. G. Zhang, J. Shen, *Nat. Commun.* **2019**, *10*, 3877.

[41] a) A. Riminucci, Z. G. Yu, M. Prezioso, R. Cecchini, I. Bergenti, P. Graziosi, V. A. Dediu, *ACS Appl. Mater. Interfaces* **2019**, *11*, 8319; b) M. Grünewald, R. Göckeritz, N. Homonnay, F. Würthner, L. W. Molenkamp, G. Schmidt, *Phys. Rev. B* **2013**, *88*, 085319.

[42] a) Y. Zhao, F. Ma, Z. H. Qu, S. Q. Yu, T. Shen, H. X. Deng, X. B. Chu, X. X. Peng, Y. B. Yuan, X. W. Zhang, J. B. You, *Science* **2022**, *377*, 531; b) Y. Bai, Z. Huang, X. Zhang, J. Lu, X. Niu, Z. He, C. Zhu, M. Xiao, Q. Song, X. Wei, C. Wang, Z. Cui, J. Dou, Y. Chen, F. Pei, H. Zai, W. Wang, T. Song, P. An, J. Zhang, J. Dong, Y. Li, J. Shi, H. Jin, P. Chen, Y. Sun, Y. Li, H. Chen, Z. Wei, H. Zhou, Q. Chen, *Science* **2022**, *348*, 747.

[43] a) J. S. Kim, J. M. Heo, G. S. Park, S. J. Woo, C. Cho, H. J. Yun, D. H. Kim, J. Park, S. C. Lee, S. H. Park, E. Yoon, N. C. Greenham, T. W. Lee, *Nature* **2022**, *611*, 688; b) C. Sun, Y. Jiang, M. Cui, L. Qiao, J. Wei, Y. Huang, L. Zhang, T. He, S. Li, H. Y. Hsu, C. Qin, R. Long, M. Yuan, *Nat. Commun.* **2021**, *12*, 2207.

[44] Y. Haruta, M. Kawakami, Y. Nakano, S. Kundu, S. Wada, T. Ikenoue, M. Miyake, T. Hirato, M. I. Saidaminov, *Chem. Mater.* **2022**, *34*, 5323.

[45] a) L. D. Li, Y. R. Wang, X. Y. Wang, R. X. Lin, X. Luo, Z. Liu, K. Zhou, S. B. Xiong, Q. Y. Bao, G. Chen, Y. X. Tian, Y. Deng, K. Xiao, J. L. Wu, M. I. Saidaminov, H. Z. Lin, C. Q. Ma, Z. S. Zhao, Y. J. Wu, L. J. Zhang, H. R. Tan, *Nat. Energy* **2022**, *7*, 708; b) D. Yang, R. X. Yang, S. Priya, S. Z. Liu, *Angew. Chem. Int. Ed.* **2019**, *58*, 4466; c) M. M. Tavakoli, K.-H. Tsui, Q. Zhang, J. He, Y. Yao, D. Li, Z. Fan, *ACS Nano* **2015**, *9*, 10287; d) S. A. Hashemi, S. Ramakrishna, A. G. Aberle, *Energy Environ. Sci.* **2020**, *13*, 685.

[46] a) Q. Chen, N. De Marco, Y. Yang, T.-B. Song, C.-C. Chen, H. Zhao, Z. Hong, H. Zhou, Y. Yang, *Nano Today* **2015**, *10*, 355; b) Y. Chen, Y. Sun, J. Peng, J. Tang, K. Zheng, Z. Liang, *Adv. Mater.* **2018**, *30*, 1703487.

[47] a) G. S. Kumar, R. R. Sumukam, R. K. Rajaboina, R. N. Savu, M. Srinivas, M. Banavoth, *ACS Appl. Energy Mater.* **2022**, *5*, 1342; b) Y. Bekenstein, B. A. Koscher, S. W. Eaton, P. Yang, A. P. Alivisatos, *J. Am. Chem. Soc.* **2015**, *137*, 16008; c) D. Chen, X. Chen, *J. Mater. Chem. C* **2019**, *7*, 1413.

[48] H. Xu, M. Wang, Z.-G. Yu, K. Wang, B. Hu, *Adv. Phys.* **2019**, *68*, 49.

[49] a) J. N. Wilson, J. M. Frost, S. K. Wallace, A. Walsh, *APL Mater.* **2019**, *7*, 010901; b) J. Yao, Q. Pan, Z.-J. Feng, Y.-A. Xiong, T.-T. Sha, H.-R. Ji, Z.-X. Gu, Y.-M. You, *APL Mater.* **2021**, *9*, 040901.

[50] a) W. Gao, X. Gao, T. A. Abtew, Y.-Y. Sun, S. Zhang, P. Zhang, *Phys. Rev. B* **2016**, *93*, 085202; b) D. O. Demchenko, N. Izyumskaya, M. Feneberg, V. Avrutin, Ü. Özgür, R. Goldhahn, H. Morkoç, *Phys. Rev. B* **2016**, *94*, 075206; c) J. Even, L. Pedesseau, J.-M. Jancu, C. Katan, *Phys. Status Solidi Rapid Res. Lett.* **2014**, *8*, 31.

[51] a) Z. G. Yu, *Sci. Rep.* **2016**, *6*, 28576; b) Z.-G. Yu, *Phys. Chem. Chem. Phys.* **2017**, *19*, 14907.

[52] W. Li, L. Zhou, O. V. Prezhdo, A. V. Akimov, *ACS Energy Lett.* **2018**, *3*, 2159.

[53] A. Fert, H. Jaffrès, *Phys. Rev. B* **2001**, *64*, 184420.

[54] K. Frohna, T. Deshpande, J. Harter, W. Peng, B. A. Barker, J. B. Neaton, S. G. Louie, O. M. Bakr, D. Hsieh, M. Bernardi, *Nat. Commun.* **2018**, *9*, 1829.

[55] S. McKechnie, J. M. Frost, D. Pashov, P. Azarhoosh, A. Walsh, M. van Schilfgaarde, *Phys. Rev. B* **2018**, *98*, 085108.

[56] J. Wang, C. Zhang, H. Liu, R. McLaughlin, Y. Zhai, S. R. Vardeny, X. Liu, S. McGill, D. Semenov, H. Guo, R. Tsuchikawa, V. V. Deshpande, D. Sun, Z. V. Vardeny, *Nat. Commun.* **2019**, *10*, 129.

[57] P. Odenthal, W. Talmadge, N. Gundlach, R. Wang, C. Zhang, D. Sun, Z.-G. Yu, Z. Valy Vardeny, Y. S. Li, *Nat. Phys.* **2017**, *13*, 894.

[58] a) J. Yin, P. Maity, L. Xu, A. M. El-Zohry, H. Li, O. M. Bakr, J.-L. Brédas, O. F. Mohammed, *Chem. Mater.* **2018**, *30*, 8538; b) S. D. Stranks, P. Plochocka, *Nat. Mater.* **2018**, *17*, 381.

[59] F. Li, J. Ding, W. Yu, X. Guan, P. Wang, D. Wu, T. Wu, *ACS Appl. Mater. Interfaces* **2020**, *12*, 3205.

[60] Y. Yang, S. Feng, Z. Li, T. Li, Y. Xiong, L. Cao, X. Gao, *J. Phys. Chem. Lett.* **2019**, *10*, 4422.

[61] S. Yang, E. Vetter, T. Wang, A. Amassian, D. Sun, *J. Phys.: Mater.* **2020**, *3*, 015012.

[62] L. Ren, Q. Zhang, Y. Tian, Y. Li, Y. Zhang, L. Zhang, S. Wang, P. Zhai, K. Jin, S. Liu, *Adv. Optical Mater.* **2023**, *11*, 2202967.

[63] C. Zhang, D. Sun, C. X. Sheng, Y. X. Zhai, K. Mielczarek, A. Zakhidov, Z. V. Vardeny, *Nat. Phys.* **2015**, *11*, 427.

[64] Y. C. Hsiao, T. Wu, M. Li, B. Hu, *Adv. Mater.* **2015**, *27*, 2899.

[65] J. Zhang, T. Wu, J. Duan, M. Ahmadi, F. Jiang, Y. Zhou, B. Hu, *Nano Energy* **2017**, *38*, 297.

[66] A. Banerjee, G. Paul, *Phys. Rev. Appl.* **2020**, *14*, 064018.

[67] R. Pan, K. Wang, Y. Li, H. Yu, J. Li, L. Xu, *Adv. Electron. Mater.* **2021**, *7*, 1900818.

[68] Y. Dou, H. Xu, Y. Liu, M. Wang, J. Zhang, O. S. Ovchinnikova, B. Hu, *Org. Electron.* **2020**, *81*, 105671.

[69] a) C. Han, H. Yu, J. Duan, K. Lu, J. Zhang, M. Shao, B. Hu, *J. Mater. Chem. C* **2018**, *6*, 6164; b) L. Deng, H. Yang, R. Pan, H. Yu, J. Li, L. Xu, K. Wang, *J. Energy Chem.* **2021**, *60*, 376.

[70] J. Zhang, B. Hu, *Nano Energy* **2020**, *76*, 104999.

[71] H. Yu, M. Wang, C. Han, K. Wang, B. Hu, *Nano Energy* **2020**, *67*, 104285.

[72] a) M. Kepenekian, R. Robles, C. Katan, D. Sapori, L. Pedesseau, J. Even, *ACS Nano* **2015**, *9*, 11557; b) Z. G. Yu, *J. Phys. Chem. Lett.* **2016**, *7*, 3078.

[73] a) K. Cong, E. Vetter, L. Yan, Y. Li, Q. Zhang, Y. Xiong, H. Qu, R. D. Schaller, A. Hoffmann, A. F. Kemper, Y. Yao, J. Wang, W. You, H. Wen, W. Zhang, D. Sun, *Nat. Commun.* **2021**, *12*, 5744; b) Z. Huang, S. R. Vardeny, T. Wang, Z. Ahmad, A. Chanana, E. Vetter, S. Yang, X. Liu, G. Galli, A. Amassian, Z. V. Vardeny, D. Sun, *Appl. Phys. Rev.* **2021**, *8*, 031408.

[74] a) D. Niesner, M. Hauck, S. Shrestha, I. Levchuk, G. J. Matt, A. Osvet, M. Batentschuk, C. Brabec, H. B. Weber, T. Fauster, *Proc. Natl. Acad. Sci. U.S.A.* **2018**, *115*, 9509; b) J. Li, P. M. Haney, *Appl. Phys. Lett.* **2016**, *109*, 193903.

[75] a) P. J. Huang, K. Taniguchi, M. Shigefuji, T. Kobayashi, M. Matsubara, T. Sasagawa, H. Sato, H. Miyasaka, *Adv. Mater.* **2021**, *33*, e2008611; b) R. Pan, X. Tang, L. Kan, Y. Li, H. Yu, K. Wang, *Nanoscale* **2023**, *15*, 3300.

[76] Y. Rakita, O. Bar-Elli, E. Meirzadeh, H. Kaslasi, Y. Peleg, G. Hodes, I. Lubomirsky, D. Oron, D. Ehre, D. Cahen, *Proc. Natl. Acad. Sci. U.S.A.* **2017**, *114*, E5504.

[77] a) M. Kim, J. Im, A. J. Freeman, J. Ihm, H. Jin, *Proc. Natl. Acad. Sci. U.S.A.* **2014**, *111*, 6900; b) T. Zhang, K. Xu, J. Li, L. He, D.-W. Fu, Q. Ye, R.-G. Xiong, *Natl. Sci. Rev.* **2023**, *10*, nwac240; c) Y. Hou, C. Wu, D. Yang, T. Ye, V. G. Honavar, A. C. T. van Duin, K. Wang, S. Priya, *J. Appl. Phys.* **2020**, *128*, 060906.

[78] K. Leng, R. L. Li, S. P. Lau, K. P. Loh, *Trends Chem.* **2021**, *3*, 716.

[79] D. Pesin, A. H. MacDonald, *Nat. Mater.* **2012**, *11*, 409.

[80] a) K. F. Mak, K. L. McGill, J. Park, P. L. McEuen, *Science* **2014**, *344*, 1489; b) D. Xiao, G. B. Liu, W. Feng, X. Xu, W. Yao, *Phys. Rev. Lett.* **2012**, *108*, 196802.

[81] S. Manzeli, D. Ovchinnikov, D. Pasquier, O. V. Yazyev, A. Kis, *Nat. Rev. Mater.* **2017**, *2*, 17033.

[82] A. Avsar, H. Ochoa, F. Guinea, B. Ozyilmaz, B. J. Van Wees, I. J. Vera-Marun, *Rev. Mod. Phys.* **2020**, *92*, 021003.

[83] D. Pesin, A. H. MacDonald, *Nat. Mater.* **2012**, *11*, 409.

[84] a) N. Tombros, C. Jozsa, M. Popinciuc, H. T. Jonkman, B. J. van Wees, *Nature* **2007**, *448*, 571; b) W. Yan, L. C. Phillips, M. Barbone, S. J. Hamalainen, A. Lombardo, M. Ghidini, X. Moya, F. Maccherozzi, S. van Dijken, S. S. Dhesi, A. C. Ferrari, N. D. Mathur, *Phys. Rev. Lett.* **2016**, *117*, 147201; c) A. Avsar, T. Y. Yang, S. Bae, J. Balakrishnan, F. Volmer, M. Jaiswal, Z. Yi, S. R. Ali, G. Guntherodt, B. H. Hong, B. Beschoten, B. Ozyilmaz, *Nano Lett.* **2011**, *11*, 2363; d) T. Y. Yang, J. Balakrishnan, F. Volmer, A. Avsar, M. Jaiswal, J. Samm, S. R. Ali, A. Pachoud, M. Zeng, M. Popinciuc, G. Guntherodt, B. Beschoten, B. Ozyilmaz, *Phys. Rev. Lett.* **2011**, *107*, 047206.

[85] a) P. J. Zomer, M. H. D. Guimarães, N. Tombros, B. J. van Wees, *Phys. Rev. B* **2012**, *86*, 161416(R) ; b) D. Huertas-Hernando, F. Guinea, A. Brataas, *Phys. Rev. Lett.* **2009**, *103*, 146801; c) C. Ertler, S. Konschuh, M. Gmitra, J. Fabian, *Phys. Rev. B* **2009**, *80*, 041405R; d) D. V. Tuan, F. Ortmann, D. Soriano, S. O. Valenzuela, S. Roche, *Nat. Phys.* **2014**, *10*, 857.

[86] a) K. Pi, W. Han, K. M. McCreary, A. G. Swartz, Y. Li, R. K. Kawakami, *Phys. Rev. Lett.* **2010**, *104*, 187201; b) D. Kochan, M. Gmitra, J. Fabian, *Phys. Rev. Lett.* **2014**, *112*, 116602.

[87] a) J.-S. Jeong, J. Shin, H.-W. Lee, *Phys. Rev. B* **2011**, *84*, 195457; b) F. Kuemmeth, S. Ilani, D. C. Ralph, P. L. McEuen, *Nature* **2008**, *452*, 448.

[88] a) F. Volmer, M. Drögeler, E. Maynicke, N. von den Driesch, M. L. Boschen, G. Güntherodt, C. Stampfer, B. Beschoten, *Phys. Rev. B* **2014**, *90*, 165403; b) H. Idzuchi, A. Fert, Y. Otani, *Phys. Rev. B* **2015**, *91*, 241407(R) ; c) M. V. Kamalakar, A. Dankert, J. Bergsten, T. Ive, S. P. Dash, *Sci. Rep.* **2014**, *4*, 6146.

[89] a) N. Tombros, A. Veligura, J. Junesch, M. H. D. Guimarães, I. J. Vera-Marun, H. T. Jonkman, B. J. van Wees, *Nat. Phys.* **2011**, *7*, 697; b) I. Neumann, J. Van de Vondel, G. Bridoux, M. V. Costache, F. Alzina, C. M. Sotomayor Torres, S. O. Valenzuela, *Small* **2013**, *9*, 156.

[90] a) J. Ingla-Aynes, R. J. Meijerink, B. J. Wees, *Nano Lett.* **2016**, *16*, 4825; b) M. Drogeler, C. Franzen, F. Volmer, T. Pohlmann, L. Banszerus, M. Wolter, K. Watanabe, T. Taniguchi, C. Stampfer, B. Beschoten, *Nano Lett.* **2016**, *16*, 3533.

[91] M. H. Guimaraes, A. Veligura, P. J. Zomer, T. Maassen, I. J. Vera-Marun, N. Tombros, B. J. van Wees, *Nano Lett.* **2012**, *12*, 3512.

[92] a) C. R. Dean, A. F. Young, I. Meric, C. Lee, L. Wang, S. Sorgenfrei, K. Watanabe, T. Taniguchi, P. Kim, K. L. Shepard, J. Hone, *Nat. Nanotechnol.* **2010**, *5*, 722; b) J. Schiefele, F. Sols, F. Guinea, *Phys. Rev. B* **2012**, *85*, 195420.

[93] J. Ingla-Aynés, M. H. D. Guimarães, R. J. Meijerink, P. J. Zomer, B. J. van Wees, *Phys. Rev. B* **2015**, *92*, 201410(R).

[94] M. Vila, J. H. Garcia, A. W. Cummings, S. R. Power, C. W. Groth, X. Waintal, S. Roche, *Phys. Rev. Lett.* **2020**, *124*, 196602.

[95] M. H. D. Guimaraes, A. Veligura, P. J. Zomer, T. Maassen, I. J. Vera-Marun, N. Tombros, B. J. van Arees, *Nano Lett.* **2012**, *12*, 3512.

[96] M. H. Guimaraes, P. J. Zomer, J. Ingla-Aynes, J. C. Brant, N. Tombros, B. J. van Wees, *Phys. Rev. Lett.* **2014**, *113*, 086602.

[97] T. Yamaguchi, Y. Inoue, S. Masubuchi, S. Morikawa, M. Onuki, K. Watanabe, T. Taniguchi, R. Moriya, T. Machida, *Appl. Phys. Express* **2013**, *6*, 073001.

[98] J. C. Leutenantsmeyer, T. Liu, M. Gurram, A. A. Kaverzin, B. J. van Wees, *Phys. Rev. B* **2018**, *98*, 125422.

[99] A. Avsar, J. Y. Tan, T. Taychatanapat, J. Balakrishnan, G. K. Koon, Y. Yeo, J. Lahiri, A. Carvalho, A. S. Rodin, E. C. O'Farrell, G. Eda, A. H. Castro Neto, B. Ozyilmaz, *Nat. Commun.* **2014**, *5*, 4875.

[100] M. Drögeler, L. Banszerus, F. Volmer, T. Taniguchi, K. Watanabe, B. Beschoten, C. Stampfer, *Appl. Phys. Lett.* **2017**, *111*, 152402.

[101] S. Liang, H. Yang, P. Renucci, B. Tao, P. Laczkowski, S. Mc-Murtry, G. Wang, X. Marie, J. M. George, S. Petit-Watelot, A. Djeffal, S. Mangin, H. Jaffres, Y. Lu, *Nat. Commun.* **2017**, *8*, 14947.

[102] A. Avsar, J. Y. Tan, M. Kurpas, M. Gmitra, K. Watanabe, T. Taniguchi, J. Fabian, B. Özyilmaz, *Nat. Phys.* **2017**, *13*, 888.

[103] a) W. Han, K. Pi, K. M. McCreary, Y. Li, J. J. Wong, A. G. Swartz, R. K. Kawakami, *Phys. Rev. Lett.* **2010**, *105*, 167202; b) W. Han, R. K. Kawakami, *Phys. Rev. Lett.* **2011**, *107*, 047207; c) Y. P. Liu, H. Idzuchi, Y. Fukuma, O. Rousseau, Y. Otani, W. S. Lew, *Appl. Phys. Lett.* **2013**, *102*, 033105.

[104] a) N. Tombros, S. Tanabe, A. Veligura, C. Jozsa, M. Popinciuc, H. T. Jonkman, B. J. van Wees, *Phys. Rev. Lett.* **2008**, *101*, 046601; b) T. Maassen, F. K. Dejene, M. H. D. Guimarães, C. Józsa, B. J. van Wees, *Phys. Rev. B* **2011**, *83*, 115410

[105] a) W. Yan, O. Txoperena, R. Llopis, H. Dery, L. E. Hueso, F. Casanova, *Nat. Commun.* **2016**, *7*, 13372; b) W. Yan, E. Sagasta, M. Ribeiro, Y. Niimi, L. E. Hueso, F. Casanova, *Nat. Commun.* **2017**, *8*, 661; c) C. K. Safeer, J. Ingla-Aynes, N. Ontoso, F. Herling, W. Yan, L. E. Hueso, F. Casanova, *Nano Lett.* **2020**, *20*, 4573.

[106] S. Singh, J. Katoch, T. Zhu, R. J. Wu, A. S. Ahmed, W. Amamou, D. Wang, K. A. Mkhoyan, R. K. Kawakami, *Nano Lett.* **2017**, *17*, 7578.

[107] M. Gurram, S. Omar, B. J. V. Wees, *Nat. Commun.* **2017**, *8*, 248.

[108] M. Gibertini, M. Koperski, A. F. Morpurgo, K. S. Novoselov, *Nat. Nanotechnol.* **2019**, *14*, 408.

[109] Z. Fei, B. Huang, P. Malinowski, W. Wang, T. Song, J. Sanchez, W. Yao, D. Xiao, X. Zhu, A. F. May, W. Wu, D. H. Cobden, J. H. Chu, X. Xu, *Nat. Mater.* **2018**, *17*, 778.

[110] a) H. Lin, F. Yan, C. Hu, Q. Lv, W. Zhu, Z. Wang, Z. Wei, K. Chang, K. Wang, *ACS Appl. Mater. Interfaces* **2020**, *12*, 43921; b) Z. Wang, D. Sapkota, T. Taniguchi, K. Watanabe, D. Mandrus, A. F. Morpurgo, *Nano Lett.* **2018**, *18*, 4303; c) S. Albarakati, C. Tan, Z. J. Chen, J. G. Partridge, G. L. Zheng, L. Farrar, E. L. H. Mayes, M. R. Field, C. G. Lee, Y. H. Wang, Y. M. Xiong, M. L. Tian, F. X. Xiang, A. R. Hamilton, O. A. Tretiakov, D. Culcer, Y. J. Zhao, L. Wang, *Sci. Adv.* **2019**, *5*, eaaw0409.

[111] W. Zhu, H. Lin, F. Yan, C. Hu, Z. Wang, L. Zhao, Y. Deng, Z. R. Kudrynskyi, T. Zhou, Z. D. Kovalyuk, Y. Zheng, A. Patane, I. Zutic, S. Li, H. Zheng, K. Wang, *Adv. Mater.* **2021**, *33*, e2104658.

[112] L. A. Benítez, J. F. Sierra, W. Savero Torres, A. Arrighi, F. Bonell, M. V. Costache, S. O. Valenzuela, *Nat. Phys.* **2018**, *14*, 303.

[113] a) J. Balakrishnan, G. Kok Wai Koon, M. Jaiswal, A. H. Castro Neto, B. Özyilmaz, *Nat. Phys.* **2013**, *9*, 284; b) F. Calleja, H. Ochoa, M. Garnica, S. Barja, J. J. Navarro, A. Black, M. M. Otrokov, E. V. Chulkov, A. Arnau, A. L. Vázquez de Parga, F. Guinea, R. Miranda, *Nat. Phys.* **2014**, *11*, 43; c) K. M. McCreary, A. G. Swartz, W. Han, J. Fabian, R. K. Kawakami, *Phys. Rev. Lett.* **2012**, *109*, 186604.

[114] a) P. Wei, S. Lee, F. Lemaitre, L. Pinel, D. Cutaia, W. Cha, F. Katmis, Y. Zhu, D. Heiman, J. Hone, J. S. Moodera, C. T. Chen, *Nat. Mater.* **2016**, *15*, 711; b) H. X. Yang, A. Hallal, D. Terrade, X. Waintal, S. Roche, M. Chshiev, *Phys. Rev. Lett.* **2013**, *110*, 046603; c) Z. Wang, D. K. Ki, H. Chen, H. Berger, A. H. MacDonald, A. F. Morpurgo, *Nat. Commun.* **2015**, *6*, 8339;

d) C. K. Safeer, N. Ontoso, J. Ingla-Aynes, F. Herling, V. T. Pham, A. Kurzmann, K. Ensslin, A. Chuvilin, I. Robredo, M. G. Vergniory, F. de Juan, L. E. Hueso, M. R. Calvo, F. Casanova, *Nano Lett.* **2019**, *19*, 8758; e) S. Omar, B. N. Madhushankar, B. J. van Wees, *Phys. Rev. B* **2019**, *100*, 155415.

[115] M. Ribeiro, S. R. Power, S. Roche, L. E. Hueso, F. Casanova, *Nat. Commun.* **2017**, *8*, 2198.

[116] a) A. Dankert, S. P. Dash, *Nat. Commun.* **2017**, *8*, 16093; b) C. K. Safeer, J. Ingla-Aynes, F. Herling, J. H. Garcia, M. Vila, N. Ontoso, M. R. Calvo, S. Roche, L. E. Hueso, F. Casanova, *Nano Lett.* **2019**, *19*, 1074.

[117] Y. Zheng, X. Ma, F. Yan, H. Lin, W. Zhu, Y. Ji, R. Wang, K. Wang, *npj 2D Materials and Applications* **2022**, *6*, 62.

[118] a) C. Wang, L. You, D. Cobden, J. Wang, *Nat. Mater.* **2023**, *22*, 542; b) Z. Guan, H. Hu, X. Shen, P. Xiang, N. Zhong, J. Chu, C. Duan, *Adv. Electron. Mater.* **2019**, *6*, 1900818; c) F. Xue, J.-H. He, X. Zhang, *Appl. Phys. Rev.* **2021**, *8*, 021316; d) M. Si, A. K. Saha, S. Gao, G. Qiu, J. Qin, Y. Duan, J. Jian, C. Niu, H. Wang, W. Wu, S. K. Gupta, P. D. Ye, *Nat. Electron.* **2019**, *2*, 580; e) J. Wu, H.-Y. Chen, N. Yang, J. Cao, X. Yan, F. Liu, Q. Sun, X. Ling, J. Guo, H. Wang, *Nat. Electron.* **2020**, *3*, 466; f) J. A. Brehm, S. M. Neumayer, L. Tao, A. O'Hara, M. Chyasnavichus, M. A. Susner, M. A. McGuire, S. V. Kalinin, S. Jesse, P. Ganesh, S. T. Pantelides, P. Maksymovych, N. Balke, *Nat. Mater.* **2020**, *19*, 43; g) F. Liu, L. You, K. L. Seyler, X. Li, P. Yu, J. Lin, X. Wang, J. Zhou, H. Wang, H. He, S. T. Pantelides, W. Zhou, P. Sharma, X. Xu, P. M. Ajayan, J. Wang, Z. Liu, *Nat. Commun.* **2016**, *7*, 12357; h) A. Belianinov, Q. He, A. Dziaugys, P. Maksymovych, E. Eliseev, A. Borisevich, A. Morozovska, J. Banys, Y. Vysochanskii, S. V. Kalinin, *Nano Lett.* **2015**, *15*, 3808.

[119] a) X. Wang, Z. Shang, C. Zhang, J. Kang, T. Liu, X. Wang, S. Chen, H. Liu, W. Tang, Y. J. Zeng, J. Guo, Z. Cheng, L. Liu, D. Pan, S. Tong, B. Wu, Y. Xie, G. Wang, J. Deng, T. Zhai, H. X. Deng, J. Hong, J. Zhao, *Nat. Commun.* **2023**, *14*, 840; b) Y. Lai, Z. Song, Y. Wan, M. Xue, C. Wang, Y. Ye, L. Dai, Z. Zhang, W. Yang, H. Du, J. Yang, *Nanoscale* **2019**, *11*, 5163; c) C. B. Park, A. Shahee, K. T. Kim, D. R. Patil, S. A. Guda, N. Ter-Oganessian, K. H. Kim, *Adv. Electron. Mater.* **2022**, *8*, 2101072.

[120] S. Deng, A. V. Sumant, V. Berry, *Nano Today* **2018**, *22*, 14.

[121] a) Z. Peng, X. Chen, Y. Fan, D. J. Srolovitz, D. Lei, *Light Sci. Appl.* **2020**, *9*, 190; b) F. Miao, S.-J. Liang, B. Cheng, *npj Quantum Materials* **2021**, *6*, 59; c) S. Z. Uddin, N. Higashitarumizu, H. Kim, E. Rabani, A. Javey, *ACS Nano* **2022**, *16*, 1339; d) A. R. Rezk, B. Carey, A. F. Chrimes, D. W. Lau, B. C. Gibson, C. Zheng, M. S. Fuhrer, L. Y. Yeo, K. Kalantar-

Zadeh, *Nano Lett.* **2016**, *16*, 849; e) S. Jiang, H. Xie, J. Shan, K. F. Mak, *Nat. Mater.* **2020**, *19*, 1295.

[122] a) Y. Wang, J. Lee, X.-Q. Zheng, Y. Xie, P. X. L. Feng, *ACS Photonics* **2019**, *6*, 3225; b) Q. H. Zhang, Y. Ying, Z. Z. Zhang, Z. J. Su, H. Ma, G. Q. Qin, X. X. Song, G. P. Guo, *Nano Lett.* **2021**, *21*, 8571; c) P. G. Steeneken, R. J. Dolleman, D. Davidovikj, F. Alijani, H. S. J. van der Zant, *2D Mater.* **2021**, *8*, 042001; d) P. Soubelet, A. A. Reynoso, A. Fainstein, K. Nogajewski, M. Potemski, C. Faugeras, A. E. Bruchhausen, *Nanoscale* **2019**, *11*, 10446; e) V. Babacic, D. Saleta Reig, S. Varghese, T. Vasileiadis, E. Coy, K. J. Tielrooij, B. Graczykowski, *Adv. Mater.* **2021**, *33*, e2008614; f) W. Yan, A. V. Akimov, M. Barra-Burillo, M. Bayer, J. Bradford, V. E. Gusev, L. E. Hueso, A. Kent, S. Kukhtaruk, A. Nadzeyka, A. Patane, A. W. Rushforth, A. V. Scherbakov, D. D. Yaremkevich, T. L. Linnik, *Nano Lett.* **2022**, *22*, 6509.

[123] R. Naaman, D. H. Waldeck, *Annu. Rev. Phys. Chem.* **2015**, *66*, 263.

[124] a) S. Dalum, P. Hedegård, *Nano Lett.* **2019**, *19*, 5253; b) R. Naaman, D. H. Waldeck, *J. Phys. Chem. Lett.* **2012**, *3*, 2178.

[125] O. Ben Dor, S. Yochelis, S. P. Mathew, R. Naaman, Y. Paltiel, *Nat. Commun.* **2013**, *4*, 2256.

[126] a) M. K. Jana, R. Song, H. Liu, D. R. Khanal, S. M. Janke, R. Zhao, C. Liu, Z. Valy Vardeny, V. Blum, D. B. Mitzi, *Nat. Commun.* **2020**, *11*, 4699; b) J. Ahn, E. Lee, J. Tan, W. Yang, B. Kim, J. Moon, *Mater. Horiz.* **2017**, *4*, 851.

[127] G. Long, R. Sabatini, M. I. Saidaminov, G. Lakhwani, A. Rasmita, X. Liu, E. H. Sargent, W. Gao, *Nat. Rev. Mater.* **2020**, *5*, 423.

[128] a) R. Pan, K. Wang, Z. G. Yu, *Mater. Horiz.* **2022**, *9*, 740; b) R. Pan, S. Tao, L. Kan, J. Hu, J. Li, Y. Li, X. Zhang, K. Wang, *Adv. Optical Mater.* **2022**, *10*, 2200064.

[129] a) C. Yuan, X. Li, S. Semin, Y. Feng, T. Rasing, J. Xu, *Nano Lett.* **2018**, *18*, 5411; b) B. Li, Y. Yu, M. Xin, J. Xu, T. Zhao, H. Kang, G. Xing, P. Zhao, T. Zhang, S. Jiang, *Nanoscale* **2023**, *15*, 1595.

[130] a) L. S. Li, Y. H. Tan, W. J. Wei, H. Q. Gao, Y. Z. Tang, X. B. Han, *ACS Appl. Mater. Interfaces* **2021**, *13*, 2044; b) C. K. Yang, W. N. Chen, Y. T. Ding, J. Wang, Y. Rao, W. Q. Liao, Y. Y. Tang, P. F. Li, Z. X. Wang, R. G. Xiong, *Adv. Mater.* **2019**, *31*, e1808088.

[131] R. G. Xiong, S. Q. Lu, Z. X. Zhang, H. Cheng, P. F. Li, W. Q. Liao, *Angew. Chem. Int. Ed.* **2020**, *59*, 9574.

[132] K. Kim, E. Vetter, L. Yan, C. Yang, Z. Wang, R. Sun, Y. Yang, A. H. Comstock, X. Li, J. Zhou, L. Zhang, W. You, D. Sun, J. Liu, *Nat. Mater.* **2023**, *22*, 322.

[133] G. Long, C. Jiang, R. Sabatini, Z. Yang, M. Wei, L. N. Quan, Q. Liang, A. Rasmita, M. Askerka, G. Walters, X. Gong, J. Xing, X. Wen, R. Quintero-Bermudez, H. Yuan, G. Xing, X. R. Wang, D. Song, O. Voznyy, M. Zhang, S. Hoogland, W. Gao, Q. Xiong, E. H. Sargent, *Nat. Photon.* **2018**, *12*, 528.

[134] R. Pan, J. Hu, S. Tao, L. Kan, H. Yu, K. Wang, *J. Mater. Chem. C* **2022**, *10*, 16706.

[135] B. Gohler, V. Hamelbeck, T. Z. Markus, M. Kettner, G. F. Hanne, Z. Vager, R. Naaman, H. Zacharias, *Science* **2011**, *331*, 894.

[136] V. Kiran, S. P. Mathew, S. R. Cohen, I. Hernandez Delgado, J. Lacour, R. Naaman, *Adv. Mater.* **2016**, *28*, 1957.

[137] C. Kulkarni, A. K. Mondal, T. K. Das, G. Grinbom, F. Tassinari, M. F. J. Mabesoone, E. W. Meijer, R. Naaman, *Adv. Mater.* **2020**, *32*, e1904965.

[138] L. Jia, C. Wang, Y. Zhang, L. Yang, Y. Yan, *ACS Nano* **2020**, *14*, 6607.

[139] Q. Qian, H. Ren, J. Zhou, Z. Wan, J. Zhou, X. Yan, J. Cai, P. Wang, B. Li, Z. Sofer, B. Li, X. Duan, X. Pan, Y. Huang, X. Duan, *Nature* **2022**, *606*, 902.

[140] M. Suda, Y. Thathong, V. Promarak, H. Kojima, M. Nakamura, T. Shiraogawa, M. Ehara, H. M. Yamamoto, *Nat. Commun.* **2019**, *10*, 2455.

[141] K. Bairagi, D. G. Romero, F. Calavalle, S. Catalano, E. Zuccatti, R. Llopis, F. Casanova, L. E. Hueso, *Adv. Mater.* **2020**, *32*, e1906908.

[142] Y. Qin, X. Gu, Y. Zhang, S. Hu, A. Guo, R. Zhang, K. Meng, T. Yang, C. Zhang, S. Lu, X. Yang, L. Guo, X. Zhu, J. Zhang, K. Lu, Z. Wei, X. Sun, *Nano Today* **2023**, *49*, 101763.

[143] H. Xu, H. Wang, J. Zhou, J. Li, *Nat. Commun.* **2021**, *12*, 4330.

[144] T. C. Song, E. Anderson, M. W. Y. Tu, K. Seyler, T. Taniguchi, K. Watanabe, M. A. McGuire, X. S. Li, T. Cao, D. Xiao, W. Yao, X. D. Xu, *Sci. Adv.* **2021**, *7*, eabg8094.

[145] T. D. Nguyen, E. Ehrenfreund, Z. V. Vardeny, *Science* **2012**, *337*, 204.

[146] J. P. Prieto-Ruiz, S. G. Miralles, H. Prima-Garcia, A. Lopez-Munoz, A. Riminucci, P. Graziosi, M. Aeschlimann, M. Cinchetti, V. A. Dediu, E. Coronado, *Adv. Mater.* **2019**, *31*, 1806817.

[147] a) S. Datta, B. Das, *Appl. Phys. Lett.* **1990**, *56*, 665; b) S. Datta, *Nat. Electron.* **2018**, *1*, 604.

[148] a) H. C. Koo, J. H. Kwon, J. Eom, J. Chang, S. H. Han, M. Johnson, *Science* **2009**, *325*, 1515; b) J. Wunderlich, B. G. Park, A. C. Irvine, L. P. Zarbo, E. Rozkotova, P. Nemec, V. Novak, J. Sinova, T. Jungwirth, *Science* **2010**, *330*, 1801; c) P. Chuang, S. C. Ho, L. W. Smith, F. Sfigakis, M. Pepper, C. H. Chen, J. C. Fan, J. P. Griffiths, I. Farrer, H. E. Beere, G. A. Jones,

D. A. Ritchie, T. M. Chen, *Nat. Nanotechnol.* **2015**, *10*, 35; d) W. Y. Choi, H. J. Kim, J. Chang, S. H. Han, H. C. Koo, M. Johnson, *Nat. Nanotechnol.* **2015**, *10*, 666.

[149] C. Betthausen, T. Dollinger, H. Saarikoski, V. Kolkovsky, G. Karczewski, T. Wojtowicz, K. Richter, D. Weiss, *Science* **2012**, *337*, 324.

[150] A. K. Geim, I. V. Grigorieva, *Nature* **2013**, *499*, 419.

[151] a) L. A. Benitez, J. F. Sierra, W. S. Torres, A. Arrighi, F. Bonell, M. V. Costache, S. O. Valenzuela, *Nat. Phys.* **2018**, *14*, 303; b) C. K. Safeer, J. Ingla-Aynes, F. Herling, J. H. Garcia, M. Vila, N. Ontoso, M. R. Calvo, S. Roche, L. E. Hueso, F. Casanova, *Nano Lett.* **2019**, *19*, 1074; c) C. K. Safeer, J. Ingla-Aynes, N. Ontoso, F. Herling, W. J. Yan, L. E. Hueso, F. Casanova, *Nano Lett.* **2020**, *20*, 4573.

[152] a) W. O. Chen, Z. Y. Sun, Z. J. Wang, L. H. Gu, X. D. Xu, S. W. Wu, C. L. Gao, *Science* **2019**, *366*, 983; b) T. C. Song, X. H. Cai, M. W. Y. Tu, X. O. Zhang, B. V. Huang, N. P. Wilson, K. L. Seyler, L. Zhu, T. Taniguchi, K. Watanabe, M. A. McGuire, D. H. Cobden, D. Xiao, W. Yao, X. D. Xu, *Science* **2018**, *360*, 1214.

[153] Z. Wang, T. Zhang, M. Ding, B. Dong, Y. Li, M. Chen, X. Li, J. Huang, H. Wang, X. Zhao, Y. Li, D. Li, C. Jia, L. Sun, H. Guo, Y. Ye, D. Sun, Y. Chen, T. Yang, J. Zhang, S. Ono, Z. Han, Z. Zhang, *Nat. Nanotechnol.* **2018**, *13*, 554.

[154] K. H. Min, D. H. Lee, S. J. Choi, I. H. Lee, J. Seo, D. W. Kim, K. T. Ko, K. Watanabe, T. Taniguchi, D. H. Ha, C. Kim, J. H. Shim, J. Eom, J. S. Kim, S. Jung, *Nat. Mater.* **2022**, *21*, 1144.

[155] S. Jiang, L. Li, Z. Wang, J. Shan, K. F. Mak, *Nat. Electron.* **2019**, *2*, 159.

[156] a) M. Cinchetti, V. A. Dediu, L. E. Hueso, *Nat. Mater.* **2017**, *16*, 507; b) S. Steil, N. Großmann, M. Laux, A. Ruffing, D. Steil, M. Wiesenmayer, S. Mathias, O. L. A. Monti, M. Cinchetti, M. Aeschlimann, *Nat. Phys.* **2013**, *9*, 242; c) M. Sun, W. Mi, *J. Mater. Chem. C* **2018**, *6*, 6619.

[157] a) L. Schulz, L. Nuccio, M. Willis, P. Desai, P. Shakya, T. Kreouzis, V. K. Malik, C. Bernhard, F. L. Pratt, N. A. Morley, A. Suter, G. J. Nieuwenhuys, T. Prokscha, E. Morenzoni, W. P. Gillin, A. J. Drew, *Nat. Mater.* **2011**, *10*, 39; b) S. Sanvito, *Nat. Phys.* **2010**, *6*, 562.

[158] J. M. De Teresa, A. Barthelemy, A. Fert, J. P. Contour, F. Montaigne, P. Seneor, *Science* **1999**, *286*, 507.

[159] S. Liang, H. Yang, H. Yang, B. Tao, A. Djeffal, M. Chshiev, W. Huang, X. Li, A. Ferri, R. Desfeux, S. Mangin, D. Lacour, M. Hehn, O. Copie, K. Dumesnil, Y. Lu, *Adv. Mater.* **2016**, *28*, 10204.

[160] T. D. Nguyen, E. Ehrenfreund, Z. V. Vardeny, *Science* **2012**, *337*, 204.

[161] D. Ciudad, M. Gobbi, C. J. Kinane, M. Eich, J. S. Moodera, L. E. Hueso, *Adv. Mater.* **2014**, *26*, 7561.

[162] D. Sun, M. Fang, X. Xu, L. Jiang, H. Guo, Y. Wang, W. Yang, L. Yin, P. C. Snijders, T. Z. Ward, Z. Gai, X. G. Zhang, H. N. Lee, J. Shen, *Nat. Commun.* **2014**, *5*, 4396.

[163] A. J. Drew, J. Hoppler, L. Schulz, F. L. Pratt, P. Desai, P. Shakya, T. Kreouzis, W. P. Gillin, A. Suter, N. A. Morley, V. K. Malik, A. Dubroka, K. W. Kim, H. Bouyanfif, F. Bourqui, C. Bernhard, R. Scheuermann, G. J. Nieuwenhuys, T. Prokscha, E. Morenzoni, *Nat. Mater.* **2009**, *8*, 109.

[164] M. Cinchetti, K. Heimer, J. P. Wustenberg, O. Andreyev, M. Bauer, S. Lach, C. Ziegler, Y. Gao, M. Aeschlimann, *Nat. Mater.* **2009**, *8*, 115.

[165] J. H. Mu, G. Z. Li, X. H. Tu, T. X. Lu, K. S. Zhao, *Chem. Phys. Lett.* **2002**, *354*, 186.

[166] a) N. Kumar, J. He, D. He, Y. Wang, H. Zhao, *Nanoscale* **2014**, *6*, 12690; b) T. Sun, C. Zhou, Z. Jiang, X. Li, K. Qiu, R. Xiao, C. Liu, Z. Ma, X. Luo, Y. Sun, Z. Sheng, *2D Mater.* **2021**, *8*, 045040; c) J. Ye, Y. Li, T. Yan, G. Zhai, X. Zhang, *J. Phys. Chem. Lett.* **2019**, *10*, 2963.

Author Photographs and Biographies

Lidan Guo is currently an associated research fellow in National Center for Nanoscience and Technology (NCNST), China. She received her Ph.D. from China University of Petroleum (Beijing) in 2020. From 2020 to 2023, Dr. Guo worked as a postdoctoral researcher in NCNST. Her current research interests mainly focus on molecular spintronics and multipurpose devices.

Shunhua Hu received his B.S. degree from Tiangong university in 2020. He is now a Ph.D. student in National Center for Nanoscience and Technology, University of Chinese Academy of Sciences under the supervision of Prof. X. Sun. His current researches focus on molecular spintronic devices and functionalities.

Xianrong Gu received her PhD from University of Chinese Academy of Sciences (UCAS) in 2022. Dr. Gu is currently a postdoctoral research follower at National Center for Nanoscience and Technology (NCNST), China. Her research interests mainly focus on the organic spintronic devices and spintronic materials.

Xiangnan Sun has been a professor and group leader at NCNST since 2016. He graduated with B.S. degree in 2003 and M.S. degree in 2006 from Qingdao University of Science and Technology. He obtained his Ph. D degree in 2011 from the Institute of Chemistry, CAS. From 2012 to 2015, he worked as postdoctoral researcher in nanodevice department at CIC nanoGUNE located in Spain. His current research interests include organic semiconductor and its electronic & spintronic applications.

Kai Wang is an associated professor at the Beijing Jiaotong University. His research is focused on the fundamental spintronics and photophysics of organic semiconductors and organic-inorganic hybrid perovskites. He was educated at the Macquarie University and the Hong Kong Polytechnic University for the Bachelor (with Honors) and Master degrees respectively. He received his PhD degree from the University of Twente, NanoElectronics Group.

Wenjing Yan is currently an Anne McLaren research fellow in the University of Nottngham, UK. She graduated with MEng degree in 2010 from the University of Oxford. She obtained her Ph. D degree in 2014 from the University of Cambridge. From 2014 to 2017, she worked as postdoctoral researcher in the Nanodevice Group at CIC nanoGUNE, Spain. From 2017 to 2019, she worked as a postdoctoral researcher in the Oxford Nano-Spin Group in the University of Oxford. Her current research interests include electronics, spintronics, optoelectronics and ultrafast optics of two-dimensional van der Waals materials and heterostructures.